Table II. Primer Sets for PCR-RFLP

Position of mutation		Primer sequences	Restriction enzyme
cDNA715	Forward	5′-CCTGGGACCTAGCAGAACACTA-3′	*Pst*I
	Reverse	5′-TGAAGAGGAGAGGGCCACAT-3′	
cDNA779	Forward	5′-CTGTTGATGTTCTTCCAGCCTCTCA-3′	*Nde*I
	Reverse	5′-TCCAGACAAGACCAACCAGCAT-3′	
cDNA829	Forward	5′-CTGTTGATGTTCTTCCAGCCTCTCA-3′	*Bsp*EI
	Reverse	5′-ATTGAAGACAGCCACCCTCC-3′	
cDNA913	Forward	5′-TAGAGGCACCACGCCTGCAT-3′	*Bgl*II
	Reverse	5′-GGTTACCAGGCCAGGGAAAGA-3′	
cDNA929	Forward	5′-TAGAGGCACCACGCCTGCAT-3′	*Stu*I
	Reverse	5′-GGAACAGGTCACTTGCGGTGTACTAG-3′	
cDNA1342	Forward	5′-CAGGTGGGACTGTGGCATTGT-3′	*Bsi*WI
	Reverse	5′-ACGCGGGTCCACAGGTTACGTA-3′	

fragment length polymorphism (RFLP) method in 67 patients. Genomic DNA could not be obtained from eight patients, who consented to the mRNA quantification and pharmacokinetic study but refused more genetic analyses. The specific primers and restriction enzymes used in this study are listed in Table II. The PCR conditions were as follows: after denaturing at 94°C for 3 min, PCR was performed with 1 μM of each primer and *Taq* DNA polymerase (Takara, Shiga, Japan), according to the following profile—94°C for 1min, 63°C for 1min, and 72°C for 1min, 35 cycles, followed by a single additional 10-min extension at 72°C. The PCR products were digested with or without apparent restriction enzymes and separated by electrophoresis on 3% agarose gel. The sequence of the *hOAT3* polymorphism (A/T913 corresponding to Ile305Phe) was confirmed by direct sequencing in heterozygotes using a multicapillary DNA sequencer RISA384 system (Shimadzu, Kyoto, Japan).

Statistical Analysis

Simple and multiple regression analyses were performed using the least-squares method. Multiple regression analyses were performed to determine the impact of the patient's characteristics on the correlation between the logarithmically transformed hOAT3 mRNA data and $Ke_{free,cez}$ or the 120-min values of the PSP test (PSP120′). In multiple regression analyses, we used $Ke_{free,cez}$ or PSP120′ as the outcome variable, and the hOAT3 mRNA level and parameters of patients as predictor variables. The nonpaired Student *t* test was used to compare groups. Statistical analyses were performed with Stat View, version 5.0 (Abacus Concepts, Berkeley, CA, USA).

Materials and Methods

Cefazolin was kindly provided by Fujisawa Pharmaceutical Co. Ltd. (Osaka, Japan). All other chemicals used were of the highest purity available.

RESULTS

The coefficient of correlation between $Ke_{free,cez}$ and C_{cr} was 0.439 ($p < 0.01$), and between $Ke_{free,cez}$ and PSP120′ it was 0.705 ($p < 0.01$) (Fig. 1A and B). As in the previous study, it was confirmed that hOAT3 mRNA level was significantly correlated with $Ke_{free,cez}$ ($r = 0.536$; $p < 0.01$) (Fig. 1C). In addition, a significant correlation between hOAT3 mRNA level and PSP120′ ($r = 0.484$; $p < 0.01$) was found (Fig. 1D).

To investigate whether the type of renal disease affects the correlation, patients were divided into Groups I (mesangial proliferative GN) and II (other renal diseases). As shown in Table I, there were no significant differences in the population between the two groups. In addition, $Ke_{free,cez}$ was significantly correlated with PSP120′ ($r = 0.723$, $p < 0.01$; Group I, $r = 0.713$, $p < 0.01$; Group II) more than C_{cr} ($r =$

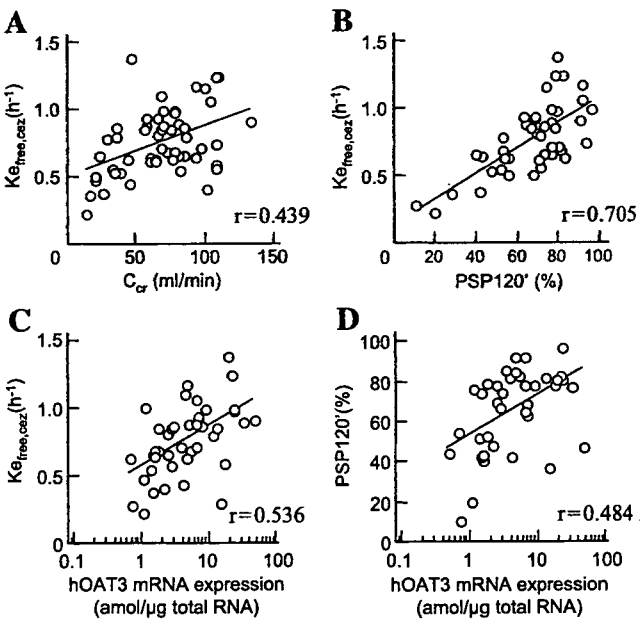

Fig. 1. The linear regression of creatinine clearance (C_{cr}) (A) or the 120-min values of the phenolsulfonphthalein test (PSP120′) (B) against the elimination rate constant for the free fraction of cefazolin ($Ke_{free,cez}$), and the linear regression between hOAT3 mRNA levels and $Ke_{free,cez}$ (C) or PSP120′ (D) in patients with renal diseases. The plasma concentration of cefazolin was measured by HPLC, and $Ke_{free,cez}$ was calculated. Total cellular RNA was extracted from the kidney biopsy specimens. The mRNA levels of hOAT3 were quantified by real-time PCR.

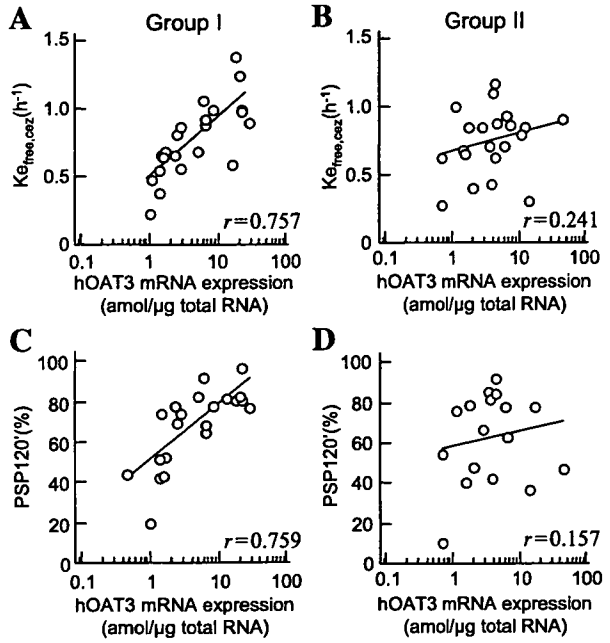

Fig. 2. The linear regression of hOAT3 mRNA levels against $Ke_{free,cez}$ (A, B) or PSP120′ (C, D) in Group I (A, C) or Group II (B, D). The plasma concentration of cefazolin was measured by HPLC, and $Ke_{free,cez}$ was calculated. Total cellular RNA was extracted from the renal biopsy specimens. The mRNA levels of hOAT3 were quantified by real-time PCR.

0.492, $p < 0.01$; Group I, $r = 0.474$, $p < 0.05$; Group II) in both groups.

Figure 2A and B shows the results of linear regression analyses with mRNA level of hOAT3 and $Ke_{free,cez}$. In Group I, the coefficient of correlation between hOAT3 mRNA level and $Ke_{free,cez}$ ($r = 0.757$; $p < 0.01$) was much higher than that in all patients. On the other hand, $Ke_{free,cez}$ was independent of hOAT3 mRNA level in Group II ($r = 0.241$; $p = 0.296$). Table III summarizes the coefficients of correlation between hOAT1–4 mRNA levels and $Ke_{free,cez}$ in each group. Although the expression level of hOAT1 mRNA was correlated with $Ke_{free,cez}$ in Group I, its coefficient was lower than the value for hOAT3. In Group II, there were no correlations between hOAT1–4 mRNA levels and $Ke_{free,cez}$. The same results were obtained between hOAT1–4 mRNA levels and PSP120′ (Fig. 2C and D, Table III).

Table III. Correlation Coefficients for $Ke_{free,cez}$, PSP120′, and the Expression Levels of hOAT mRNAs in Group I and Group II

	Group I		Group II	
mRNA expression	$Ke_{free,cez}$	PSP120′	$Ke_{free,cez}$	PSP120′
hOAT1	0.558[a]	0.556[a]	0.267	0.391
hOAT2	0.051	0.083	0.387	0.213
hOAT3	0.757[a]	0.759[a]	0.241	0.157
hOAT4	0.183	0.186	0.247	0.474

Values represent coefficients of the correlation between mRNA expression of hOATs and $Ke_{free,cez}$ or PSP120′.
[a] Each mRNA level of hOAT is significantly correlated with $Ke_{free,cez}$ or PSP120′.

Table IV. Multiple Regression Analyses for $Ke_{free,cez}$ or PSP120′

	r Value	
+ Additional parameters	$Ke_{free,cez}$	PSP120′
hOAT3 mRNA level + age	0.603	0.526
hOAT3 mRNA level + aspartate aminotransferase	0.585	0.558
hOAT3 mRNA level + alanine aminotransferase	0.543	0.534
hOAT3 mRNA level + lactate dehydrogenase	0.530	0.497

To assess whether personal profiles of patients and liver functions affect the correlation between hOAT3 mRNA level and $Ke_{free,cez}$, simple or multiple linear regression analyses were performed using gender, age, aspartate aminotransferase (AST), alanine aminotransferase (ALT), and lactate dehydrogenase (LDH). Coefficients of correlation were not improved by dividing the subjects into males and females ($r = 0.450$, $p < 0.01$; males, $r = 0.600$, $p < 0.01$; females). Table IV shows the results of multiple linear regression analyses. Age and liver functions did not improve the correlation. In addition, the same results were observed for PSP120′.

Next, we investigated six SNPs in coding regions (cSNPs) with nonsynonymous changes in the *hOAT3* gene of 67 patients, because some cSNPs in the *hOAT3* gene were considered to affect the transport activity independent of the expression level. In the *hOAT3* gene, one nonsynonymous polymorphism (A913 was replaced with T) was detected via the PCR-RFLP method and confirmed by direct sequencing (Table V, Fig. 3). This polymorphism resulted in an amino acid substitution; Ile305 was changed to Phe (Ile305Phe). The allele frequency of cDNA 913 was 95.5% for allele A and 4.5% for allele T. However, there was no remarkable difference in $Ke_{free,cez}$ or PSP120′ between the two genotypic groups (Table V). Furthermore, the coefficient of correlation between hOAT3 mRNA level and $Ke_{free,cez}$ ($r = 0.551$, $p < 0.01$) or PSP120′ ($r = 0.493$, $p < 0.01$) was not changed by excluding patients with this variant.

DISCUSSION

Recent insights into the mechanisms of progressive renal dysfunction have indicated that tubulointerstitial pathology does not simply follow glomerular injury and that tubular cells may be the primary targets for various pathophysiological influences (16). Among each type of renal disease, the cause and pathway of progression are different (11–13). For each type of renal disease, renal transporters are assumed regulated in a different manner. Therefore, it may be important to consider types of renal disease when assessing the correlation between pharmacokinetics and expression levels of transporters. In the present study, we found a good relationship between the hOAT3 mRNA level and the rate of elimination of cefazolin in patients with mesangial proliferative GN (Group I), which is the most common form of primary renal disease (17). It was postulated that hOAT3 expression levels directly regulated the rate of elimination of

Table V. hOAT3 Genetic Variants in Patients with Renal Diseases and Phenotypic Indexes (n = 67)

Location	Position	Allele	Effect	Allele frequency	Genotype	Frequency (%)	$Ke_{free,cez}$ (h^{-1})	PSP120′ (%)
Exon5	cDNA715	C	239Gln	67 (100.0%)	C/C	100.0		
		T	239Stop	0 (0.0%)	C/T	0.0		
					T/T	0.0		
Exon6	cDNA779	T	260Ile	67 (100.0%)	T/T	100.0		
		G	260Arg	0 (0.0%)	T/G	0.0		
					G/G	0.0		
Exon6	cDNA829	C	277Arg	67 (100.0%)	C/C	100.0		
		T	277Trp	0 (0.0%)	C/T	0.0		
					T/T	0.0		
Exon7	cDNA913	A	305Ile	64 (100.0%)	A/A	91.0	0.75 ± 0.25	66.1 ± 20.5
		T	305Phe	3 (4.5%)	A/T	9.0	0.84 ± 0.29	64.2 ± 15.6
					T/T	0.0		
Exon7	cDNA929	C	310Ala	67 (100.0%)	C/C	100.0		
		T	310Val	0 (0.0%)	C/T	0.0		
					T/T	0.0		
Exon10	cDNA1342	G	448Val	67 (100.0%)	G/G	100.0		
		A	448Ile	0 (0.0%)	G/A	0.0		
					A/A	0.0		

Variance is indicated as the mean ± SD.

cefazolin in these patients. The level of hOAT1 mRNA was also correlated with $Ke_{free,cez}$ in Group I. However, its correlation coefficient was lower than the coefficient between hOAT3 mRNA levels and $Ke_{free,cez}$. In addition, transport of cefazolin by hOAT1 was negligible in our previous study (10,18). Therefore, it was considered that elimination rate of cefazolin was affected by the expression level of hOAT3 rather than hOAT1.

On the other hand, in Group II, there was no significant correlation between the mRNA level of hOAT3 and the rate of elimination of cefazolin. It is suggested that additional factors are affecting the rate. One possibility is that hOAT3 is regulated by a posttranslational mechanism in these patients. For example, the activation of protein kinase C (PKC) inhibited the uptake of anionic compounds by OAT3 in intact renal proximal tubules and cells stably expressing OAT3 (19). It was recently reported by Soodvilai *et al.* (20,21) that tyrosine kinase, phosphatidylinositol 3-kinase, mitogen-activated protein kinase, protein kinase A, and mitogen-activated/extracellular signal-regulated kinase kinase were involved in epidermal growth factor signaling pathways, which could affect the function of OAT3. Group II included patients with diabetic nephropathy, and the PKC activity of renal tubular cells was reported to be increased in the diabetic state (22,23). Thus, it is possible that the function of hOAT3 is modified by various kinases in some patients of Group II. However, the signaling pathways in proximal tubules specific for each renal disease, such as lupus nephritis or interstitial nephritis, are little understood in contrast to those in the glomeruli. Further studies should be performed to clarify the posttranslational regulation of tubular transporters in renal disease.

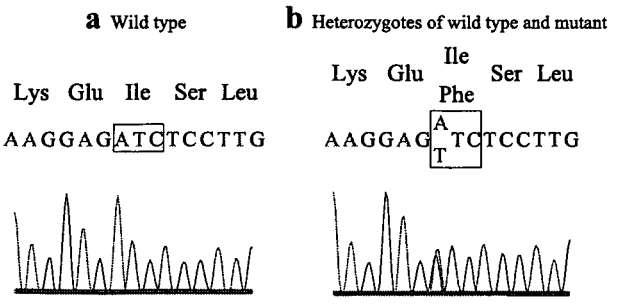

Fig. 3. Electropherograms of the SLC22A8 gene sequence in the region around the A913T mutation.

Poor correlations between C_{cr} and the renal clearance of drugs have been reported (4,5). In the present study, C_{cr} was not a good predictor of $Ke_{free,cez}$ (Fig. 1), indicating that C_{cr} can not be used to accurately assess anionic drug excretion. Alternatively, it has been indicated that tubular function should be considered when making precise adjustments of dosage. However, tubular function is not routinely evaluated in the clinical setting. In the present study, hOAT3 mRNA level was significantly correlated with PSP120′ in the patients with mesangial proliferative GN (Fig. 2). PSP is almost completely excreted into urine in the unchanged form (24,25) and in a substrate of hOAT3 (10). It is suggested that PSP tests are good predictors of the renal elimination rate of drugs, which are transported by hOAT3, with less invasive methods. Markers for the expression level of individual transporters from urine or blood will be useful to predict the rate of elimination of substrate drugs.

Genetic polymorphisms of drug transporters as well as drug-metabolizing enzymes affect the pharmacokinetics of drugs. Ishikawa *et al.* (26) suggested that cSNPs of transporter genes are responsible for the variation in responses to drugs among individuals. For example, SNPs of human organic anion transporting polypeptides (OATP-C, SLC21A6) were reported to influence the pharmacokinetics of pravastatin (27–29). In the present study, we screened for six cSNPs of the *hOAT3* gene, and found one polymorphism, Ile305Phe (allelic frequency, 4.5%). However, no pharmacokinetic significance of this cSNP was apparent. Nishizato *et al.* (28) also reported that a polymorphism in the *hOAT3* gene,

T723A (Ala389Val), was unlikely to be associated with differences in the clearance of pravastatin. Thus, it is likely that cSNPs of *hOAT3* do not account for variation in the rate of elimination in most cases, and that the expression level of hOAT3 is more important to explain the interindividual variation in the elimination rates of cefazolin and PSP than cSNPs in patients with renal diseases.

There are several differences in substrate specificity between hOAT1 and hOAT3. hOAT3, but not hOAT1, transports estrone sulfate (ES), and the cationic drug famotidine (30,31). Renal elimination rates of these substrates may also be affected by hOAT3 expression levels. While methotrexate was transported by both hOAT1 and hOAT3 (32), aciclovir and ganciclovir were transported by hOAT1 but not hOAT3 (33). It is assumed that the urinary excretion of these drugs is affected by hOAT1 expression levels.

In conclusion, the expression level of hOAT3 mRNA was suggested to be a significant pharmacokinetics marker in predicting the rate of elimination of anionic drugs in patients with mesangial proliferative GN.

ACKNOWLEDGMENTS

This work was supported by a grant-in-aid for Comprehensive Research on Aging and Health from the Ministry of Health and Welfare of Japan (H15-Choju-006), by a grant-in-aid for Scientific Research from the Ministry of Education, Culture, Sports, Science, and Technology of Japan, by a grant-in-aid from the Japan Research Foundation for Clinical Pharmacology, and by the 21st Century COE program "Knowledge Information Infrastructure for Genome Science."

REFERENCES

1. L. Dettli. Drug dosage in renal disease. *Clin. Pharmacokinet.* **1**:126–134 (1976).
2. O. Shemesh, H. Golbetz, J. P. Kriss, and B. D. Myers. Limitations of creatinine as a filtration marker in glomerulopathic patients. *Kidney Int.* **28**:830–838 (1985).
3. Y. Urakami, N. Kimura, M. Okuda, and K. Inui. Creatinine transport by basolateral organic cation transporter hOCT2 in the human kidney. *Pharm. Res.* **21**:976–981 (2004).
4. R. Hori, K. Okumura, A. Kamiya, H. Nihira, and H. Nakano. Ampicillin and cephalexin in renal insufficiency. *Clin. Pharmacol. Ther.* **34**:792–798 (1983).
5. S. E. Tett, C. M. Kirkpatrick, A. S. Gross, and A. J. McLachlan. Principles and clinical application of assessing alterations in renal elimination pathways. *Clin. Pharmacokinet.* **42**:1193–1211 (2003).
6. J. B. Pritchard and D. S. Miller. Mechanisms mediating renal secretion of organic anions and cations. *Physiol. Rev.* **73**:765–796 (1993).
7. K. Inui and M. Okuda. Cellular and molecular mechanisms of renal tubular secretion of organic anions and cations. *Clin. Exp. Nephrol.* **2**:100–108 (1998).
8. K. Inui, S. Masuda, and H. Saito. Cellular and molecular aspects of drug transport in the kidney. *Kidney Int.* **58**:944–958 (2000).
9. B. C. Burckhardt and G. Burckhardt. Transport of organic anions across the basolateral membrane of proximal tubule cells. *Rev. PhysioL, Biochem. Pharmacol.* **146**:95–158 (2003).
10. Y. Sakurai, H. Motohashi, H. Ueo, S. Masuda, H. Saito, M. Okuda, N. Mori, M. Matsuura, T. Doi, A. Fukatsu, O. Ogawa, and K. Inui. Expression levels of renal organic anion transporters (OATs) and their correlation with anionic drug excretion in patients with renal diseases. *Pharm. Res.* **21**:61–67 (2004).
11. R. E. Gilbert and M. E. Cooper. The tubulointerstitium in progressive diabetic kidney disease: more than an aftermath of glomerular injury? *Kidney Int.* **56**:1627–1637 (1999).
12. M. H. Park, V. D'Agati, G. B. Appel, and C. L. Pirani. Tubulointerstitial disease in lupus nephritis: relationship to immune deposits, interstitial inflammation, glomerular changes, renal function, and prognosis. *Nephron* **44**:309–319 (1986).
13. E. Alexopoulos, D. Seron, R. B. Hartley, and J. S. Cameron. Lupus nephritis: correlation of interstitial cells with glomerular function. *Kidney Int.* **37**:100–109 (1990).
14. H. Motohashi, Y. Sakurai, H. Saito, S. Masuda, Y. Urakami, M. Goto, A. Fukatsu, O. Ogawa, and K. Inui. Gene expression levels and immunolocalization of organic ion transporters in the human kidney. *J. Am. Soc. Nephrol.* **13**:866–874 (2002).
15. I. Yano, T. Ito, M. Takano, and K. Inui. Evaluation of renal tubular secretion and reabsorption of levofloxacin in rats. *Pharm. Res.* **14**:508–511 (1997).
16. K. A. Nath. The tubulointerstitium in progressive renal disease. *Kidney Int.* **54**:992–994 (1998).
17. J. Floege and J. Feehally. IgA nephropathy: recent developments. *J. Am. Soc. Nephrol.* **11**:2395–2403 (2000).
18. H. Ueo, H. Motohashi, T. Katsura, K. Inui. Human organic anion transporter hOAT3 is a potent transporter of cephalosporin antibiotics, in comparison with hOAT1. *Biochem. Pharmacol.* **70**:1104–1113 (2005).
19. M. Takeda, T. Sekine, and H. Endou. Regulation by protein kinase C of organic anion transport driven by rat organic anion transporter 3 (rOAT3). *Life Sci.* **67**:1087–1093 (2000).
20. S. Soodvilai, V. Chatsudthipong, K. K. Evans, S. H. Wright, and W. H. Dantzler. Acute regulation of OAT3-mediated estrone sulfate transport in isolated rabbit renal proximal tubules. *Am. J. Physiol. Renal. Physiol.* **287**:F1021–F1029 (2004).
21. S. Soodvilai, S. H. Wright, W. H. Dantzler, V. Chatsudthipong. Involvement of tyrosine kinase and PI3K in the regulation of OAT3-mediated estrone sulfate transport in isolated rabbit renal proximal tubules. *Am. J. Physiol. Renal. Physiol.* in press.
22. D. Koya and G. L. King. Protein kinase C activation and the development of diabetic complications. *Diabetes* **47**:859–866 (1998).
23. S. H. Park, H. J. Choi, J. H. Lee, C. H. Woo, J. H. Kim, and H. J. Han. High glucose inhibits renal proximal tubule cell proliferation and involves PKC, oxidative stress, and TGF-beta 1. *Kidney Int.* **59**:1695–1705 (2001).
24. J. V. Moller and M. I. Sheikh. Renal organic anion transport system: pharmacological, physiological, and biochemical aspects. *Pharmacol. Rev.* **34**:315–358 (1982).
25. G. R. Brown. Cephalosporin–probenecid drug interactions. *Clin. Pharmacokinet.* **24**:289–300 (1993).
26. T. Ishikawa, A. Tsuji, K. Inui, Y. Sai, N. Anzai, M. Wada, H. Endou, and Y. Sumino. The genetic polymorphism of drug transporters: functional analysis approaches. *Pharmacogenomics* **5**:67–99 (2004).
27. C. Marzolini, R. G. Tirona, and R.B. Kim. Pharmacogenomics of the OATP and OAT families. *Pharmacogenomics* **5**:273–282 (2004).
28. Y. Nishizato, I. Ieiri, H. Suzuki, M. Kimura, K. Kawabata, T. Hirota, H. Takane, S. Irie, H. Kusuhara, Y. Urasaki, A. Urae, S. Higuchi, K. Otsubo, and Y. Sugiyama. Polymorphisms of OATP-C (SLC21A6) and OAT3 (SLC22A8) genes: consequences for pravastatin pharmacokinetics. *Clin. Pharmacol. Ther.* **73**:554–565 (2003).
29. M. Niemi, E. Schaeffeler, T. Lang, M. F. Fromm, M. Neuvonen, C. Kyrklund, J. T. Backman, R. Kerb, M. Schwab, P. J. Neuvonen, M. Eichelbaum, and K. T. Kivisto. High plasma pravastatin concentrations are associated with single nucleotide polymorphisms and haplotypes of organic anion transporting polypeptide-C (OATP-C, SLCO1B1). *Pharmacogenetics* **14**:429–440 (2004).
30. S. H. Cha, T. Sekine, J. I. Fukushima, Y. Kanai, Y. Kobayashi,

T. Goya, and H. Endo. Identification and characterization of human organic anion transporter 3 expressing predominantly in the kidney. *Mol. Pharmacol.* **59**:1277–1286 (2001).
31. H. Motohashi, Y. Uwai, K. Hiramoto, M. Okuda, and K. Inui. Different transport properties between famotidine and cimetidine by human renal organic ion transporters (SLC22A). *Eur. J. Pharmacol.* **503**:25–30 (2004).
32. Y. Uwai, R. Taniguchi, H. Motohashi, H. Saito, M. Okuda, and K. Inui. Methotrexate–loxoprofen interaction: involvement of human organic anion transporters hOAT1 and hOAT3. *Drug Metab. Pharmacokinet.* **19**:369–374 (2004).
33. M. Takeda, S. Khamdang, S. Narikawa, H. Kimura, Y. Kobayashi, T. Yamamoto, S. H. Cha, T. Sekine, and H. Endou. Human organic anion transporters and human organic cation transporters mediate renal antiviral transport. *J. Pharmacol. Exp. Ther.* **300**:918–924 (2002).

ORGANIC LETTERS

2006
Vol. 8, No. 4
613−616

Unequivocal Synthesis of (*Z*)-Alkene and (*E*)-Fluoroalkene Dipeptide Isosteres To Probe Structural Requirements of the Peptide Transporter PEPT1

Ayumu Niida,[†] Kenji Tomita,[†] Makiko Mizumoto,[†] Hiroaki Tanigaki,[†] Tomohiro Terada,[‡] Shinya Oishi,[†] Akira Otaka,[†,§] Ken-ichi Inui,[‡] and Nobutaka Fujii*,[†]

Graduate School of Pharmaceutical Sciences, Kyoto University, Sakyo-ku, Kyoto 606-8501, Japan, Department of Pharmacy, Kyoto University Hospital, Sakyo-ku, Kyoto 606-8507, Japan, and Graduate School of Pharmaceutical Sciences, The University of Tokushima, Tokushima 770-8505, Japan

nfujii@pharm.kyoto-u.ac.jp

Received November 17, 2005

ABSTRACT

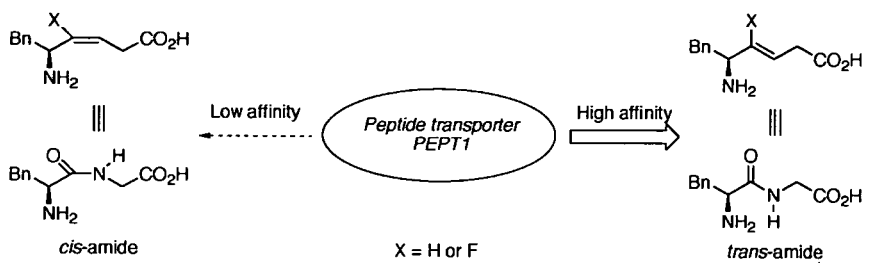

Described is a novel synthetic route for dipeptide isosteres containing (*Z*)-alkene and (*E*)-fluoroalkene units as *cis*-amide bond equivalents via organocopper-mediated reduction of γ-acetoxy- or γ,γ-difluoro-α,β-unsaturated-δ-lactams. The synthesized isosteres were evaluated in terms of their affinities for the peptide transporter PEPT1. *trans*-Amide isosteres tended to possess higher affinities for PEPT1 as compared to the corresponding *cis*-amide bond equivalents.

In postgenomic drug discovery research, the rapid elucidation of structural requirements of the ligands for newly identified drug targets (e.g., GPCRs, enzymes, transporters, etc.) is strongly needed in the arena of medicinal chemistry.[1] Many protein drug targets interact with proteinic or peptidic ligands. Therefore, development of peptidomimetic small molecules is important for investigating criteria for the mutual molecular recognition.[2] Alkene-type dipeptide isosteres represent potential amide bond mimetics (Figure 1).[3] Fluoroalkene dipeptide isosteres were designed as electrostatically favorable mimetics as compared to simple alkene isosteres.[4] These isosteres have structural similarities with the parent peptides

† Graduate School of Pharmaceutical Sciences, Kyoto University.
‡ Kyoto University Hospital.
§ The University of Tokushima.

(1) (a) Drews, J. *Science* **2000**, *287*, 1960. (b) Klabunde, T.; Hessler, G. *ChemBioChem* **2002**, *3*, 928. (c) Tyndall, J. D. A.; Pfeiffer, B.; Abbenante, G., Fairlie, D. P. *Chem. Rev.* **2005**, *105*, 793.

(2) (a) Burgess, K. *Acc. Chem. Res.* **2001**, 34, 826. (b) Bursavich M. G.; Rich, D. H. *J. Med. Chem.* **2002**, *45*, 541. (c) Hruby, V. J. *J. Med Chem.* **2003**, *46*, 4215.

(3) (a) Oishi, S.; Kamano, T.; Niida, A.; Odagaki, Y.; Hamanaka, N.; Yamamoto, M.; Ajito, K.; Tamamura, H.; Otaka, A.; Fujii, N. *J. Org. Chem.* **2002**, *67*, 6162. (b) Wipf, P.; Xiao, J. *Org. Lett.* **2005**, *7*, 103. (c) Xiao, J.; Weisblum, B.; Wipf, P. *J. Am. Chem. Soc.* **2005**, *127*, 5742.

(4) (a) Abraham, R. J.; Ellison, S. L. R.; Schonholzer, P.; Thomas, W. A. *Tetrahedron* **1986**, *42*, 2101. (b) Allmendinger, T.; Furet, P.; Hungerbühler, E.; *Tetrahedron Lett.* **1990**, *31*, 7297. (c) Allmendinger, T.; Furet, P.; Hungerbühler, E.; *Tetrahedron Lett.* **1990**, *31*, 7301. (d) Otaka, A.; Watanabe, J.; Yukimasa, A.; Sasaki, Y.; Watanabe, H.; Kinoshita, T.; Oishi, S.; Tamamura, H.; Fujii, N. *J. Org. Chem.* **2004**, *69*, 1634. (e) V. d. Veken, P.; Senten, K.; Kertèsz, I.; D. Meester, I.; Lambeir, A.-M.; Maes, M.-B.; Scharpè, S.; Haemers, A.; Augustyns, K. *J. Med. Chem.* **2005**, *48*, 1768. (f) Nakamura, Y.; Okada, M.; Sato, A.; Horikawa, H.; Koura, M.; Saito, A.; Taguchi, T. *Tetrahedron* **2005**, *61*, 5741.

10.1021/ol052781k CCC: $33.50
Published on Web 01/24/2006

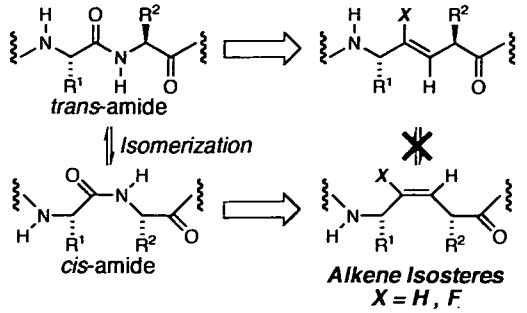

Figure 1. *Cis/trans* equilibrium of peptide bond and the corresponding alkene- or fluoroalkene isosteres.

and resist enzymatic degradation. Peptide bonds exist in *cis/trans* equilibrium, while alkene isosteres serve as defined *trans*-amide or *cis*-amide equivalents, which do not isomerize to each other. *Cis/trans* isomerization of peptide bonds (especially Xaa-Pro sequences) in several bioactive peptides tends to play an important role in their conformations and biological activities.[5] Therefore, alkene and fluoroalkene isosteres might be promising tools for conformational analysis of bioactive peptides and proteins.[6] We have been engaged in the development of synthetic methodologies for (*E*)-alkene or (*Z*)-fluoroalkene dipeptide isosteres as *trans*-amide bond equivalents utilizing organocopper reagents or SmI_2. However, the lack of efficient synthetic methodologies for the preparation of (*Z*)-alkene or (*E*)-fluoroalkene dipeptide isosteres as *cis*-amide bond equivalents has limited an extensive application of alkene and fluoroalkene isosteres in the analysis of amide bond geometries in bioactive peptides and proteins. In this paper, we describe a new synthetic approach for the preparation of (*Z*)-alkene or (*E*)-fluoroalkene dipeptide isosteres. We also include the application of these isosteres to probe structural requirements of the peptide transporter PEPT1.

Our synthetic routes for the preparation of (*Z*)-alkene and (*E*)-fluoroalkene isosteres are depicted in Scheme 1. We envisioned key synthetic intermediates **B** would be synthesized by organocopper-mediated reduction of lactam **A** with predominant formation of β,γ-(*Z*)-alkenes or (*E*)-fluoroalkenes as *cis*-amide equivalents. This strategy could be expanded into consecutive one-pot reduction/α-alkylation methodologies for the synthesis of structurally diverse α-alkylated (*Z*)-alkene and (*E*)-fluoroalkene dipeptide isosteres.[7] First, we synthesized γ-acetoxy- or γ,γ-difluoro-α,β-unsaturated lactams and examined the organocopper-mediated reduction of these substrates to confirm whether this approach was applicable to the synthesis of *cis*-amide bond isosteres.

Guibé et al. reported a similar but inherently different convergent approach to the synthesis of (*Z*)-alkene isosteres

Scheme 1. Synthetic Route for (*Z*)-Alkene and (*E*)-Fluoroalkene Dipeptide Isosteres

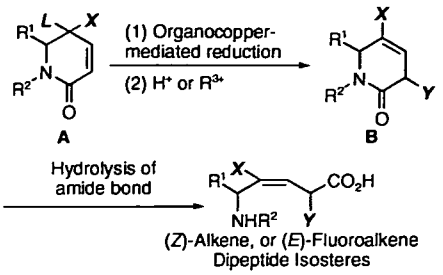

L: leaving group (OAc or F). *X*: H or F. *Y*: H or R^3.

via 3,6-dihydropyridin-2-ones, in which the β,γ-(*Z*)-alkene unit was constructed by Grubbs' RCM after condensation of chiral allylamines with chiral vinyl acetic acids.[8] The present method provides a new entity for the synthesis of (*Z*)-alkene isosteres in a divergent fashion. That is complementary to their method as well as our alternative method based on organocoper-mediated *anti*-S_N2' reaction.[9] It is noteworthy that to our knowledge, this is the first unequivocal synthesis of (*E*)-fluoroalkene dipeptide isosteres.

Substrates for the organocopper-mediated reduction were synthesized by the sequence of reactions shown in Scheme 2. Synthesis of acetate **6** started from a known phenylalanine derivative **1**.[9] Conversion of the *N*-protecting group of **1** to *N*-Ns (Ns = 2-nitrobenzenesulfonyl)[10] followed by *O*-protection with a TBS group gave *N*-Ns amide derivative **2**. Treatment of **2** with DMB (2,4-dimethoxybenzyl) alcohol under Mitsunobu conditions afforded the *N*-DMB sulfonamide **3**. After removal of the *N*-Ns group of **3**, acylation of the resulting secondary amine followed by *O*-TBS deprotection gave the acrylamide derivative **4**. RCM reaction of **4** with Grubbs' ruthenium catalyst[11] proceeded smoothly at room temperature to yield the γ-hydroxy-α,β-unsaturated δ-lactam **5**. Lactam **5** was converted to acetate **6** by Ac_2O treatment in the presence of pyridine.

γ,γ-Difluoro-α,β-unsaturated δ-lactam **12** was synthesized from the β-amino ester **10**, which was prepared from phenylacetaldehyde **7** and the chiral amine **8** via rhodium catalized diastereoselective Reformatsky–Honda reaction.[4d,12] After DIBAL-H treatment of **10**, (*Z*)-selective Horner–Wadsworth–Emmons reaction[13] of the resulting aldehyde gave (*Z*)-enoate **11** in 72% yield with a concomitant formation of small amount of (*E*)-isomer (4%). After deprotection of the Boc and *t*-Bu groups of **11** using 4 M HCl in dioxane, cyclization with EDC gave the desired lactam **12**.

(5) Dugave, C.; Demange, L. *Chem. Rev.* **2003**, *103*, 2475.
(6) Wang, X. J.; Xu, B.; Mullins, A. B.; Neiler, F. K.; Etzkorn, F. A. *J. Am. Chem. Soc.* **2004**, *126*, 15533.
(7) Otaka, A.; Watanabe, H.; Yukimasa, A.; Oishi, S.; Tamamura, H.; Fujii, N. *Tetrahedron Lett.* **2001**, *42*, 5443, and references cited thererin.
(8) Boucard, V.; S.-Dorizon, H.; Guibé, F. *Tetrahedron* **2002**, *58*, 7275.
(9) Niida, A.; Oishi, S.; Sasaki, Y.; Mizumoto, M.; Tamamura, H.; Fujii, N.; Otaka, A. *Tetrahedron Lett.* **2005**, *46*, 4183.
(10) Fukuyama, T.; Jow, C.-K.; Cheung, M. *Tetrahedron Lett.* **1995**, *36*, 6373.
(11) Scholl, M.; Ding, S.; Lee, C. W.; Grubbs, R. H. *Org. Lett.* **1999**, *1*, 953.
(12) Honda, T.; Wakabayashi, H.; Kanai, K. *Chem. Pharm. Bull.* **2002**, *50*, 307.
(13) Ando, K.; Oishi, T.; Hirama, M.; Ohno, H.; Ibuka, T. *J. Org. Chem.* **2000**, *65*, 4745.

Scheme 2. Synthesis of Requisite Substrates for Organocopper-Mediated Reduction

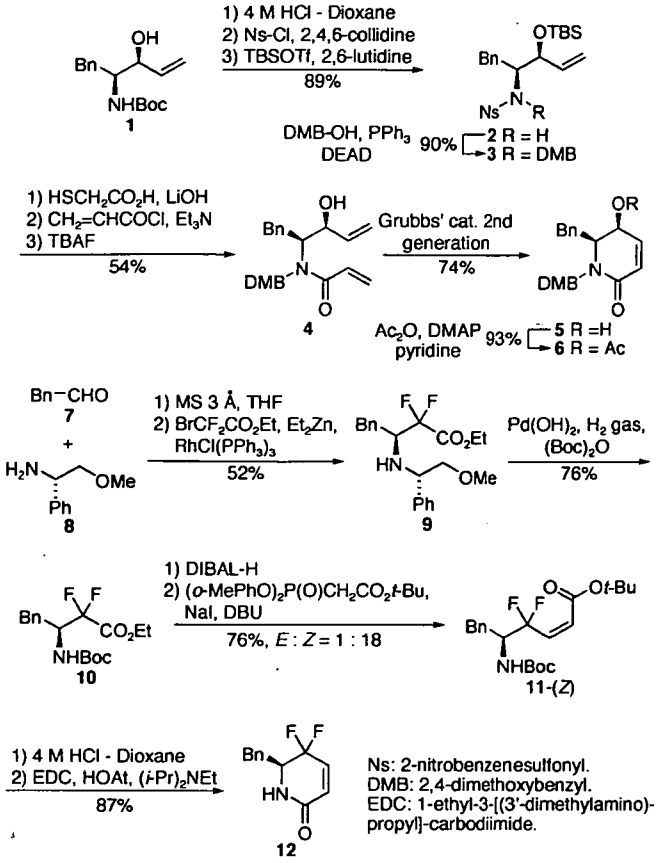

Next we examined the organocopper-mediated reduction of lactams **6** and **12** (Scheme 3). The reaction of acetate **6** with Me_3CuLi_2·LiI·3LiBr[14] proceeded smoothly at −78 °C to yield the β,γ-unsaturated lactam **13** in a good yield (88%). The DMB group of lactam **13** was easily removed using TFA. Treatment of difluorolactam **12** with Me_3CuLi_2·LiI·3LiBr also gave the desired reduction product **15** in excellent yield (92%).

Scheme 3. Synthesis of Phe-Gly Type (Z)-Alkene- and (*E*)-Fluoroalkene Dipeptide Isosteres via Organocopper-Mediated Reduction of Lactams **6** and **12**

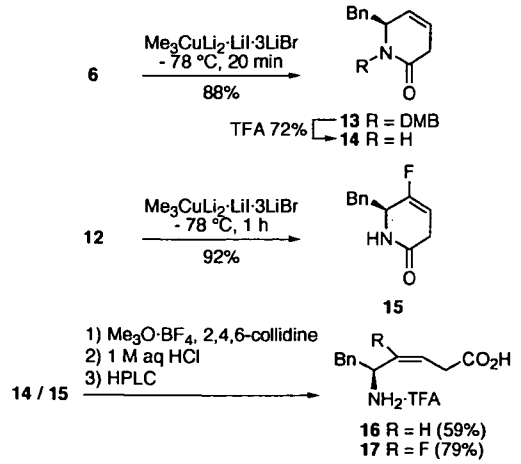

Next, we carried out the hydrolysis of the amide bond in lactams **14** and **15** to accomplish the synthesis of the *cis*-amide bond isosteres. Lactams **14** and **15** were converted to lactim ethers using $Me_3O{\cdot}BF_4$. Hydrolysis of the lactim ethers[15] under acidic conditions followed by HPLC purification using 0.1% TFA aqueous MeCN gave Phe-Gly type (*Z*)-alkene dipeptide isostere (Phe-ψ[(*Z*)-CH=CH]-Gly **16**) and (*E*)-fluoroalkene dipeptide isostere (Phe-ψ[(*E*)-CF=CH]-Gly **17**),[16] respectively as TFA salts.

The above organocopper-mediated reduction is applicable to consecutive one-pot α-alkylation (Scheme 4). After reduction of lactam **6** with Me_3CuLi_2·LiI·3LiBr, the resulting metal enolate was trapped by Bn-Br to yield the *trans*-α-substituted diketopiperazine mimetic **18** as a main product. After deprotection of the DMB group using TFA, the resulting lactam **19** was subjected to ring-opening followed by *N*-Boc protection to yield Boc-L-Phe-ψ[(*Z*)-CH=CH]-D-Phe-OMe **20** in 40% yield with a small amount of α-epimerized product (13%). Boc-D-Phe-ψ[(*E*)-CF=CH]-L-Phe-OMe **23** was also synthesized from lactam **21** by a procedure

Scheme 4. Synthesis of α-Substituted (*Z*)-Alkene and (*E*)-Fluoroalkene Dipeptide Isosteres Utilizing Organocopper-Mediated Reduction−Alkylation

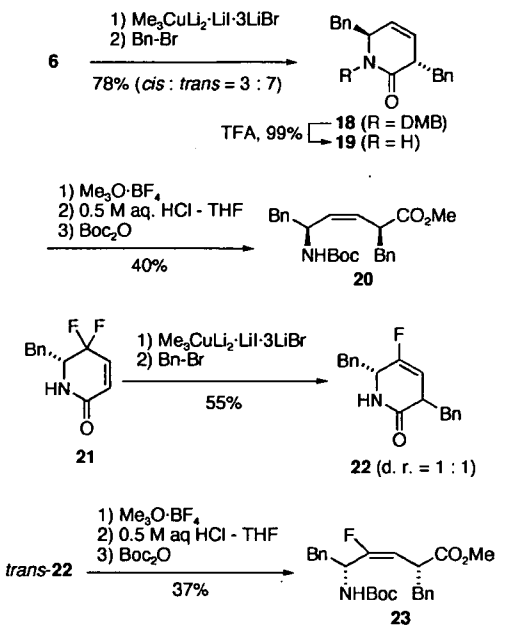

(14) Single electron transfer (SET) mechanism has been proposed as one of the plausible mechanisms of organocopper-mediated reduction. The electron-transfer potency of Me_3CuLi_2 was proved to be higher than that of the corresponding Gilman-type reagent such as Me_2CuLi. See: Chounan, Y.; Horino, H.; Ibuka, T.; Yamamoto, Y. *Bull. Chem. Soc. Jpn.* **1997**, *70*, 1953.

(15) Schöllkopf, U.; Hartwig, W.; Pospischil, K.-H.; Kehne, H. *Synthesis* **1981**, 966.

(16) Coupling constants of **17** and **23** ($^3J_{HF}$ = 20.7 and 20.5 Hz, respectively) are consistent with those of α-fluorovinyl groups possessing a (*E*)-configuration ($^3J_{HFtrans}$ = 18−22 Hz). See ref 4b.

similar to that for the synthesis of isostere **20**.[17] Precise stereocontrol and introduction of other functional groups at the α-position are under investigation.

Next, we investigated whether the di/tri-peptide transporter, PEPT1 recognized synthetic Phe-Gly type isosteres as substrates. PEPT1 is a membrane protein which has 12 transmembrane domains and mediates intestinal uptake of not only di-/tripeptides but also several drugs structually related to small peptides such as β-lactam antibiotics.[18] Structure−activity relationship studies of various substrates for PEPT1 have been carried out in order to apply this transporter to develop orally bio-available drugs. However precise recognition mechanisms have not been elucidated. We envisioned that alkene dipeptide isosteres would be useful tools for analysis of recognition mechanisms of PEPT1 because of their structural similarity to parent dipeptides. We also expected that the potency of dipeptide isosteres as amide bond mimetics could be evaluated by use of the PEPT1 dipeptide transport system.

The bioactivities of synthetic Phe-Gly isosteres for PEPT1 were determined by the inhibition of [^{3}H]Gly-Sar uptake in PEPT1-expressing Caco-2 cell in comparison with *trans*-amide type isosteres, **24**, **25**, and other related compounds (see the Supporting Information attached). Inhibition constants (K_i) of parent dipeptide Phe-Gly and its isosteres are shown in Table 1. *trans*-Amide equivalents **24** and **25** possessed good affinity for PEPT1 corresponding to the parent dipeptide (K_i: Phe-Gly, 0.205 mM; **24**, 0.853 mM; **25**, 1.34 mM). It is of note that affinities of the *cis*-amide equivalents **16** and **17** for PEPT1 were more than 10 times weaker than those of *trans*-isomers. These data suggest that PEPT1 predominantly recognizes *trans*-amide conformations of dipeptides. This is in good accordance with the previous report by Brandsch et al., in which PEPT1 recognized *trans*-conformation of Ala-ψ[CS−N]-Pro.[19] Conformationally flexible analogues **26** and **27** retained moderate affinity in comparison with *cis*-amide equivalents. Presumably, analogues **26** and **27** could exist as *trans*-amide-like conformers, which were favorable for the interaction with PEPT1, due to their flexibility. Contrary to our expectation, an increase of affinity by the introduction of fluoroalkene unit was not observed (**24** vs **25**). Further investigation is required for verification of the effect of fluorine as a carbonyl oxygen mimic.

Table 1. K_i Values of Phe-Gly and Various Isosteres Based on Inhibition of [^{3}H]Gly-Sar Uptake by PEPT1 in Caco-2 Cell

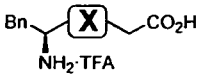

compd	X	K_i (mM)
Phe-Gly	−CO-NH−	0.205
16	−ψ[(*Z*)-CH=CH]−	>10.0
17	−ψ[(*E*)-CF=CH]−	>10.0
24	−ψ[(*E*)-CH=CH]−	0.853
25	−ψ[(*Z*)-CF=CH]−	1.34
26	−ψ[CH_2-CH_2]−	2.17
27	−ψ[CF_2-CH_2]−	1.67

In conclusion, we presented a novel unambiguous synthetic route for the syntheses of (*Z*)-alkene and (*E*)-fluoroalkene dipeptide isosteres as *cis*-amide bond mimetics via organocopper-mediated reduction of γ-acetoxy- or γ,γ-difluoro-α,β-unsaturated δ-lactams. We also carried out comparative studies of affinities for peptide transpoter PEPT1 between the *cis*-amide mimetics and the corresponding *trans*-amide isosteres, and found that peptide transporter PEPT1 predominantly recognizes *trans*-amide bond conformations in dipeptides. Synthetic studies on various α-substituted (*E*)-fluoroalkene isosteres and further structure−activity-relationship studies on dipeptide mimetics for PEPT1 are currently proceeding.

Acknowledgment. We thank Dr. Terrence R. Burke, Jr., NCI, NIH, for proofreading this manuscript. This research was supported in part by 21st Century COE Program "Knowledge Information Infrastructure for Genome Science", a Grant-in-Aid for Scientific Research from the Ministry of Education, Culture, Sports, Science and Technology, Japan, the Japan Society for the Promotion of Science (JSPS), and the Japan Health Science Foundation. A.N. is grateful for Research Fellowships from the JSPS for Young Scientists.

Supporting Information Available: Synthesis of compounds **24**−**27**. Experimental procedures and spectral data. This material is available free of charge via the Internet at http://pubs.acs.org.

OL052781K

(17) In ^{1}H NMR experiments, α-protons (position-3) of 3,6-*trans* isomers such as **18** or *trans*-**22** appeared upfield from the corresponding α-protons of 3,6-*cis* isomeres. See ref 9.

(18) (a) Våbenø, J.; Lejon, T.; Nielsen, C. U.; Steffansen, B.; Chen, W.; Ouyang, H.; Borchardt, R. T.; Luthman, K. *J. Med. Chem.* **2004**, *47*, 1060. (b) Våbenø, J.; Nielsen, C. U.; Ingebrigtsen, T.; Lejon, T.; Steffansen, B.; Luthman, K. *J. Med. Chem.* **2004**, *47*, 4755. (c) Terada, T.; Inui, K. *Curr. Drug Metab.* **2004**, *5*, 85. (d) Biegel, A.; Gebauer, S.; Hartrodt, B.; Brandsh, M.; Neubert, K.; Thondorf, I. *J. Med. Chem.* **2005**, *48*, 4410.

(19) Brandsh, M.; Thunecke, F.; Küllertz, G.; Schutkowski, M.; Fischer, G.; Neubert, K. *J. Biol. Chem.* **1998**, *273*, 3861.

Pflugers Arch - Eur J Physiol (2006) 452: 64–70
DOI 10.1007/s00424-005-0005-x

EPITHELIAL TRANSPORT

Megumi Irie · Tomohiro Terada · Masahiro Tsuda · Toshiya Katsura · Ken-ichi Inui

Prediction of glycylsarcosine transport in Caco-2 cell lines expressing PEPT1 at different levels

Received: 20 June 2005 / Accepted: 22 September 2005 / Published online: 10 November 2005

Abstract H^+-coupled peptide transporter 1 (PEPT1) and the basolateral peptide transporter mediate the absorption of small peptides and peptide-like drugs in the small intestine. Recently, we constructed a mathematical model to simulate glycylsarcosine (Gly-Sar) transport in Caco-2 cells. In this study, we attempted to adjust our model to a change in the expression level of PEPT1. To obtain cell lines expressing PEPT1 at different levels, recloning of Caco-2 cells was performed, and nine clones were isolated. Compared with parental cells, clones 1 and 9 exhibited the lowest and the highest levels of [^{14}C]Gly-Sar uptake from the apical side, respectively, whereas activities of the basolateral peptide transporter were comparable. Kinetic analysis demonstrated that the difference in the activity of PEPT1 was accounted by variations in V_{max}. Moreover, PEPT1 mRNA level was positively related to the activity of [^{14}C]Gly-Sar uptake (r=0.55). Based on these findings, the V_{max} value of PEPT1 was defined as a variable using the amount of PEPT1 mRNA as an index of the expression level. With this improved model, Gly-Sar transport in clones 1 and 9 was well-predicted, suggesting that our model can simulate Gly-Sar transport in cells expressing PEPT1 at different levels.

Keywords Peptide transporter · Small intestine · Absorption · Simulation · Expression level

Abbreviations PEPT1: H^+-coupled peptide transporter 1 · Gly-Sar: glycylsarcosine

M. Irie · T. Terada · M. Tsuda · T. Katsura · K.-i. Inui (✉)
Department of Pharmacy,
Kyoto University Hospital,
Faculty of Medicine,
Kyoto University,
Sakyo-ku,
606-8507 Kyoto, Japan
e-mail: inui@kuhp.kyoto-u.ac.jp
Tel.: +81-75-7513577
Fax: +81-75-7514207

Introduction

H^+-coupled peptide transporter 1 (PEPT1) expressed in brush-border membranes of intestinal epithelial cells transports dipeptides and tripeptides from the lumen into cells by utilizing an inward H^+ gradient and mediates the absorption of dipeptides and tripeptides [1, 6, 14, 23]. Because of its broad substrate specificity, PEPT1 can accept various peptide-like drugs, such as oral β-lactam antibiotics and the anticancer agent bestatin; therefore, PEPT1 serves as a drug transporter [7, 23, 29]. On the other hand, it has been demonstrated that another peptide transporter is expressed in the basolateral membrane [10, 12, 19, 24, 26, 27]. The basolateral peptide transporter mediates the extrusion of substrates taken up by PEPT1 into the circulation and is involved in the absorption of peptide-like drugs.

Recently, based on the influx and efflux properties of PEPT1 and the basolateral peptide transporter, we constructed a computational model of glycylsarcosine (Gly-Sar) transport in Caco-2 cells [11]. This model was composed of three compartments (i.e., the apical, cellular, and basolateral compartments) and two functional factors (PEPT1 and the basolateral peptide transporter). To reproduce the saturation of both transporters, the rate constants of Gly-Sar transport by PEPT1 and the basolateral peptide transporter were defined as variables using the respective kinetic parameters K_m and V_{max}. With this model, the time course of Gly-Sar transport at various concentrations in the absorptive direction could be predicted well, indicating that the model could be used to underlie a simulator to forecast the absorption of peptide-like drugs in the small intestine. However, the expression level of PEPT1 was presumed to be constant and was not incorporated into this model as a variable factor, although the expression level of PEPT1 differed from the segment of the intestine [17] and the intestinal PEPT1 was regulated by various factors, such as food, hormones, drugs, and diurnal rhythm [2, 23]. It is, therefore, essential to enable the model to achieve a change in the expression level of PEPT1 for the development of a simulator of drug absorption in the small intestine.

In the present study, we first performed the recloning of Caco-2 cells for two purposes: (1) to isolate clones appropriate for assessment of the improved model, and (2) to investigate the relation between transport activity and the expression level of PEPT1. Based on the findings of uptake studies and the quantification of PEPT1 mRNA, we defined the amount of PEPT1 mRNA as an index for the expression level of PEPT1, and we described mathematically the maximal velocity (V_{max}) of PEPT1. Furthermore, using two clones differing in the expression level of PEPT1, validation of the improved model of Gly-Sar transport was performed.

Materials and methods

Materials

[^{14}C]Gly-Sar (4.07 GBq/mmol) was obtained from Moravek Biochemicals, Inc. (Brea, CA, USA) and D-[1-^{3}H(N)] mannitol (629 GBq/mmol) was from NEN Life Science Products, Inc. (Boston, MA, USA). Gly-Sar was purchased from Sigma Chemical Co. (St. Louis, MO, USA). All other chemicals used were of the highest purity available.

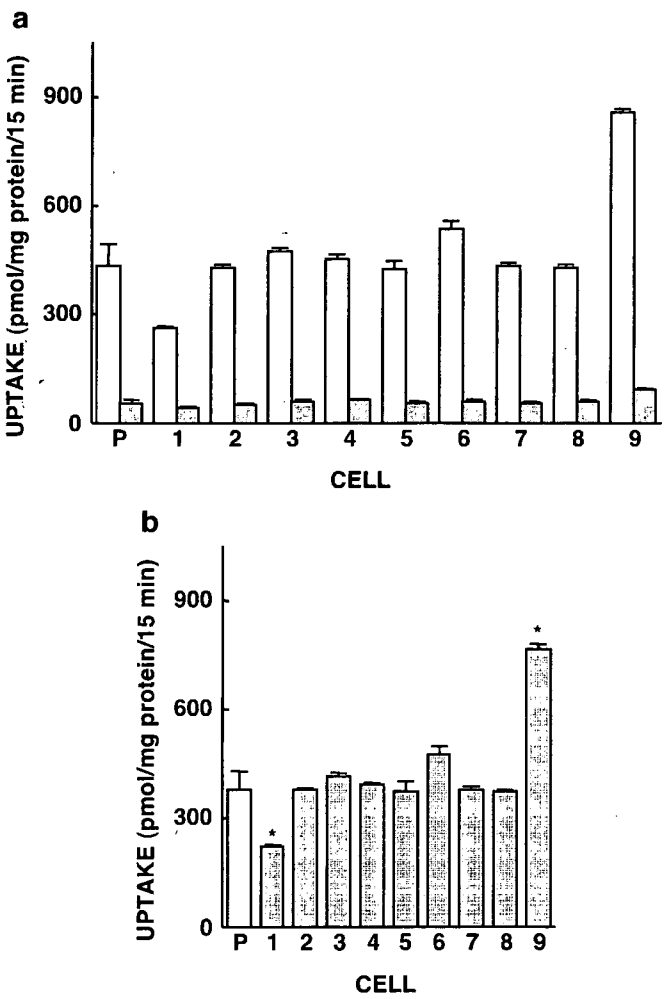

Fig. 1 [^{14}C]Gly-Sar uptake from the apical side in the parental Caco-2 cells (*P*) and in the nine cell lines (*clones 1–9*) cloned from Caco-2 cells. **a** The cell monolayers were incubated at 37°C for 15 min with an incubation medium containing 20 μM [^{14}C]Gly-Sar (pH 6.0) in the absence (*open column*) or in the presence (*hatched column*) of 10 mM unlabeled Gly-Sar. After washing, the radioactivity of dissolved cells was measured. **b** The specific uptake of PEPT1 was calculated by subtracting the uptake in the presence of 10 mM Gly-Sar from that in its absence. Each column represents the mean ± SE of six independent monolayers from two separate experiments. *P<0.05, significantly different from the parental Caco-2 cells

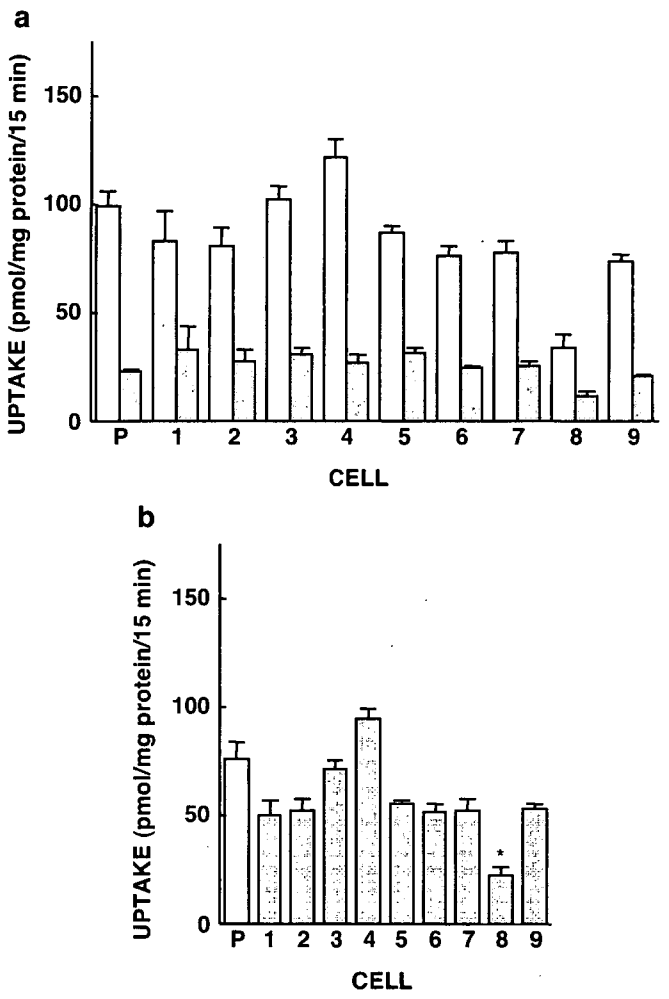

Fig. 2 [^{14}C]Gly-Sar uptake from the basolateral side in the parental Caco-2 cells (*P*) and in the nine cell lines (*clones 1–9*) cloned from Caco-2 cells. **a** The cell monolayers were incubated at 37°C for 15 min with the incubation medium containing 20 μM [^{14}C]Gly-Sar (pH 6.0) in the absence (*open column*) or in the presence (*hatched column*) of 10 mM unlabeled Gly-Sar. After washing, the radioactivity of dissolved cells was measured. **b** The specific uptake of PEPT1 was calculated by subtracting the uptake in the presence of 10 mM Gly-Sar from that in its absence. Each column represents the mean ± SE of six independent monolayers from two separate experiments. *P<0.05, significantly different from the parental Caco-2 cells

Cell culture and recloning of Caco-2 cells

Caco-2 cells at passage 18, obtained from the American Type Culture Collection (ATCC HTB37), were maintained by serial passage in plastic culture dishes, as described previously [12]. To measure the uptake of [^{14}C]Gly-Sar from the apical or basolateral side, Caco-2 cells were seeded on 12-well cluster plates (1×10^4 cells/well, 1 ml of culture medium) or on microporous membrane filters (3.0-μm pores, 1 cm^2) inside Transwell cell culture chambers (Costar, Cambridge, MA, USA) at a cell density of 6.6×10^4 cells/filter, respectively. Each Transwell chamber was filled with 0.33 and 1 ml of culture medium in the apical and basolateral compartments, respectively. For transepithelial transport studies, Caco-2 cells were seeded on microporous membrane filters (3.0-μm pores, 4.7 cm^2) at a density of 3×10^5 cells/filter and cultured with 1.5 and 2.6 ml of culture medium on the apical and basolateral sides, respectively. To prepare total RNA from the cells, Caco-2 cells were seeded on 35-mm plastic dishes (2×10^4 cells/dish, 2 ml of culture medium). Cell monolayers were given a fresh culture medium every 2–4 days and were used on the 14th or 15th day for experiments.

To obtain cell lines with different expression levels of PEPT1, parental Caco-2 cells at passage 38 were seeded on 100-mm plastic dishes at a density of 1×10^2 cells/dish. Between 3 and 4 weeks, single colonies appeared and nine colonies were picked up for subsequent experiments. In the present study, parental and cloned Caco-2 cells were used between passages 41 and 48.

Uptake and transport studies with cell monolayers

The uptake of [^{14}C]Gly-Sar from the apical or basolateral side was determined and transport studies were performed as described previously [21, 24]. Briefly, Caco-2 cells were preincubated with 2 ml of the incubation medium (pH 7.4) on both the apical and the basolateral sides for 10 min, and then 2 ml of 20 μM [^{14}C]Gly-Sar, including 0.5 μCi/ml [^{3}H]mannitol (pH 6.0) or the incubation medium (pH 7.4), was added to the apical or basolateral side, respectively. After incubation for the indicated period at 37°C, accumulation and transepithelial transport of [^{14}C]Gly-Sar and [^{3}H]mannitol were determined by liquid scintillation counting.

Quantification of PEPT1 mRNA expression

The expression levels of PEPT1 mRNA were determined by real-time polymerase chain reaction (PCR), as described previously [16]. Briefly, aliquots of 0.5 μg of total RNA, isolated from original Caco-2 cells and from each clone using the RNeasy Mini Kit (Qiagen, Hilden, Germany), were reverse-transcribed in 20 μl of reaction mixture. Real-time PCR was performed in a total volume of 20 μl containing 0.05 μg of cDNA, 1 μM forward and reverse primers, 0.2 μM TaqMan probe, and 10 μl of TaqMan Universal PCR Master Mix (Applied Biosystems, Foster City, CA, USA) under the following conditions: 50 cycles of 94°C for 15 s and 60°C for 60 s. The primer/probe set for the specific amplification of PEPT1 (accession no. NM_005703) was designed according to parameters incorporated in the Primer Express software (PE Biosystems, Foster City, CA, USA). The forward and reverse primers were ATTGTGTCGCTCTCCATTGTCTAC (positions 306–329) and ATGACCTCACAGACCACAACCAT (positions 389–367), respectively. The sequence of TaqMan probe was TTGGACAAGCAGTCACCTCAGTAAGCT CCA, corresponding to positions 334–363.

Data analysis

Each experimental point represents the mean ± SE of three to nine measurements from one to three separate experiments. Data from uptake studies were analyzed statistically by one-way analysis of variance followed by Sheffé's test. Kinetic parameters of isolated clones were statistically compared with those of parental cells by nonpaired *t* test.

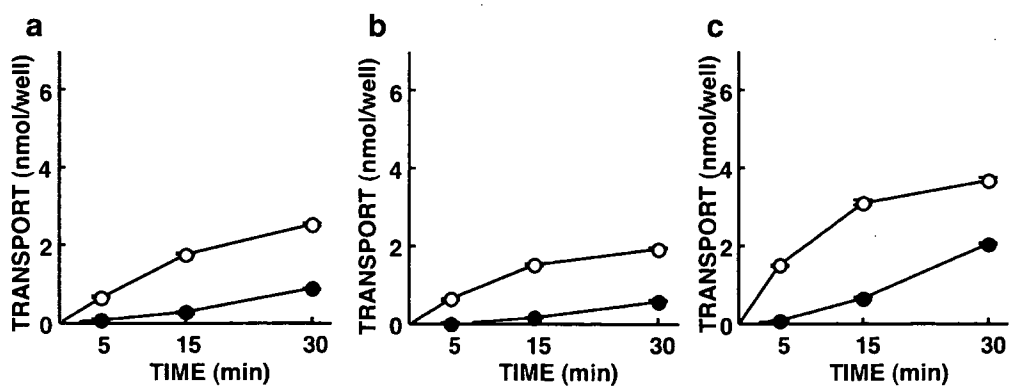

Fig. 3 [^{14}C]Gly-Sar transport from the apical side in the parental Caco-2 cells (**a**), in clone 1 (**b**), and in clone 9 (**c**). After preincubation, the cell monolayers were incubated at 37°C with 20 μM [^{14}C]Gly-Sar (pH 6.0) containing [^{3}H]mannitol, and the incubation medium (pH 7.4) was added to the apical and basolateral sides, respectively. At the indicated time, the accumulation (*circle*) and the transepithelial transport (*filled circle*) of [^{14}C]Gly-Sar were determined. The radioactivity of [^{3}H]mannitol was measured simultaneously for validation of paracellular flux (not shown). Each *symbol* represents the mean ± SE of three independent monolayers. When *error bars* are not shown, they are smaller than the *symbols*

Results

[^{14}C]Gly-Sar uptake from apical and basolateral sides in parental Caco-2 cells and in nine clones obtained by recloning of Caco-2 cells

It has been reported that Caco-2 cells, which are a useful model of intestinal epithelial cells, are heterogeneous [28]. Therefore, recloning of the parental Caco-2 cells was performed to obtain a series of cell lines differing in the expression level of PEPT1; nine clones were isolated. Compared with the parental Caco-2 cells, [^{14}C]Gly-Sar uptake from the apical side in clone 1 was markedly lower, whereas that in clone 9 was about twofold (Fig. 1). The other seven clones exhibited activity for the uptake of [^{14}C]Gly-Sar comparable to that of the parental Caco-2 cells. On the other hand, [^{14}C]Gly-Sar uptake from the basolateral side in all the clones except clone 8 did not differ significantly from that in the parental Caco-2 cells: clone 8 cells exhibited less activity (Fig. 2).

Transepithelial transport of [^{14}C]Gly-Sar in parental Caco-2 cells and in clones 1 and 9

Uptake studies suggested that two clones (clones 1 and 9) may be useful for the assessment of the transepithelial transport of Gly-Sar because the expression level of PEPT1 in each clone is different from that in the parental Caco-2 cells and because the activities of the basolateral peptide transporter in these cells are comparable. We then examined Gly-Sar transport in the absorptive direction of these cells. As shown in Fig. 3, the transepithelial transport and the accumulation of [^{14}C]Gly-Sar in clones 1 and 9 were less and greater than those in the Caco-2 cells, respectively. On the other hand, permeation of [^{3}H]mannitol, which is an index of paracellular flux, did not differ in these cells (data not shown). Results demonstrated that the intensity of PEPT1 activity obviously affects not only the accumulation but also the transepithelial transport of substrates.

Table 1 Michaelis–Menten constant (K_m) and the maximal velocity (V_{max}) of [^{14}C]Gly-Sar uptake by PEPT1 in the parental Caco-2 cells, in clone 1, and in clone 9

Cell line	Kinetic parameters	
	K_m (mM)	V_{max} (nmol/mg protein per 15 min)
Parental Caco-2	1.04±0.08	14.2±0.23
Clone 1	0.93±0.15	10.3±0.43*
Clone 9	0.98±0.11	33.0±2.64*

[^{14}C]Gly-Sar uptake from the apical side in each cell line was measured at various concentrations for 15 min, and then the kinetic parameters were determined by nonlinear least squares regression analysis according to the Michaelis–Menten equation. Each value represents the mean ± SE of three independent experiments
*P<0.05, significantly different from the value of the parental cells

Kinetic analysis of [^{14}C]Gly-Sar uptake by PEPT1

Next, we performed a kinetic analysis of [^{14}C]Gly-Sar uptake from the apical side in the parental cells and in clones 1 and 9. As illustrated in Fig. 4, [^{14}C]Gly-Sar uptake in these cells was saturable, and kinetic parameters were estimated according to the Michaelis–Menten equation using nonlinear least squares regression analysis. As summarized in Table 1, the maximal velocity (V_{max}) of [^{14}C]Gly-Sar uptake in clones 1 and 9 was significantly lower and greater than that in the parental Caco-2 cells, respectively. However, Michaelis–Menten constants (K_m) were comparable among these cells. These findings suggested that the differences in the activities of [^{14}C]Gly-Sar uptake among the three cell lines are caused by the different expression levels of PEPT1 protein.

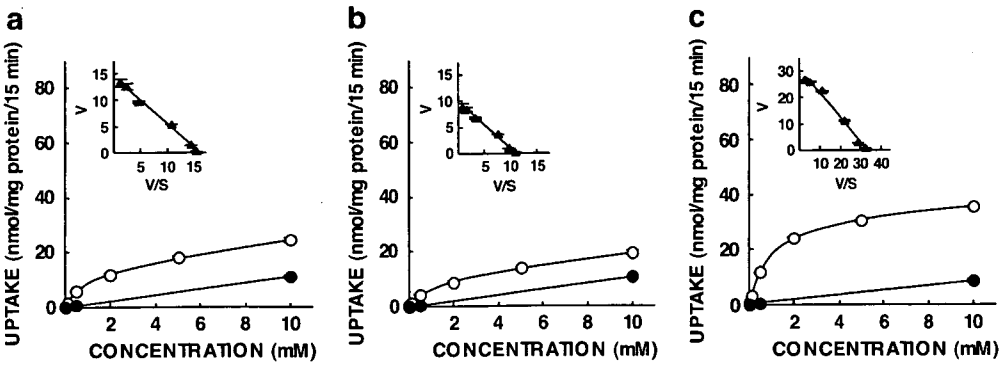

Fig. 4 Concentration dependence of [^{14}C]Gly-Sar uptake from the apical side in the parental Caco-2 cells (**a**), in clone 1 (**b**), and in clone 9 (**c**). [^{14}C]Gly-Sar uptake was measured at various concentrations for 15 min in the absence (*circle*) or in the presence (*filled circle*) of 50 mM glycyl-leucine. These figures show the representative data of three experiments. Each *point* represents the mean ± SE of three monolayers. When *error bars* are not shown, they are smaller than the *symbols*. *Insets*: Eadie–Hofstee plots of [^{14}C]Gly-Sar uptake after correction for nonspecific component (*filled triangle*). *V* Uptake rate (nmol/mg protein per 15 min), *S* [^{14}C]Gly-Sar concentration (mM)

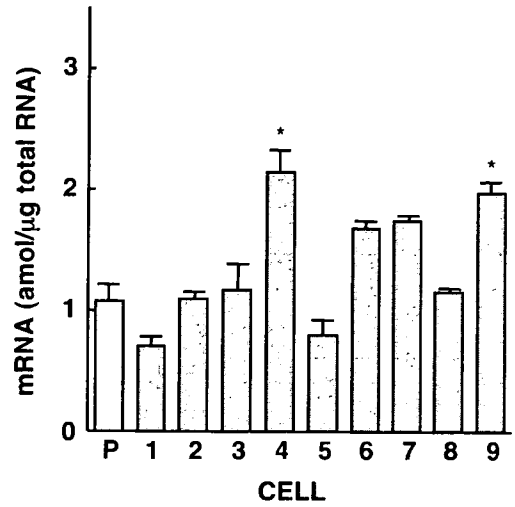

Fig. 5 Quantification of PEPT1 mRNA expressed in the parental Caco-2 cells (*P*) and in the nine cell lines (*clones 1–9*). Total cellular RNA was extracted from the cells and then reverse-transcribed. The mRNA levels of PEPT1 in these cells were determined by real-time PCR using an ABI Prism 7700 sequence detector. Each column represents the mean ± SE of five to eight independent monolayers from two or three separate experiments. **P*<0.05, significantly different from the parental Caco-2 cells

Expression levels of PEPT1 mRNA in parental Caco-2 cells and in isolated clones

Moreover, the amount of PEPT1 mRNA expressed in the parental Caco-2 cells and in the nine clones was determined by real-time PCR. As shown in Fig. 5, the expression level of PEPT1 mRNA in clone 1 was lower than that in the parental cells. In contrast, clone 9 displayed a level of expression that was higher than that of the parental Caco-2 cells. These findings were consistent with the activity of [^{14}C]Gly-Sar uptake from the apical side in these cells (Fig. 1). On the other hand, clone 4 exhibited a greater level of PEPT1 mRNA expression, despite activities of PEPT1 comparable to those of the parental Caco-2 cells.

To further examine whether the expression level of PEPT1 mRNA can serve as an indicator of PEPT1 activity, the correlation between the uptake of [^{14}C]Gly-Sar and the amount of PEPT1 mRNA was investigated in the parental and cloned cells at passages 41 and 46 in order to increase the number of samples. Figure 6 shows the linear regression of the activity of [^{14}C]Gly-Sar uptake from the apical side against the expression level of PEPT1 mRNA in the parental Caco-2 cells and in the nine clones. A positive linear correlation was observed with r=0.55.

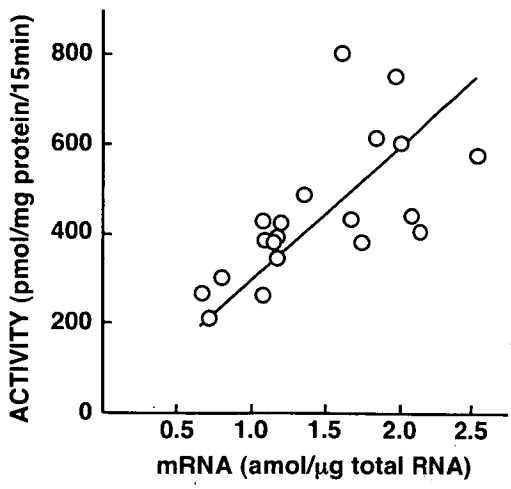

Fig. 6 The linear regression of the activity of [^{14}C]Gly-Sar uptake against the expression level of PEPT1 mRNA in the parental Caco-2 cells and in the nine clones. [^{14}C]Gly-Sar uptake was measured experimentally, and the amount of PEPT1 mRNA was determined by real-time PCR in the same batch of the respective cells. Each *symbol* was plotted using the mean of [^{14}C]Gly-Sar uptake and that of mRNA expression in three independent monolayers

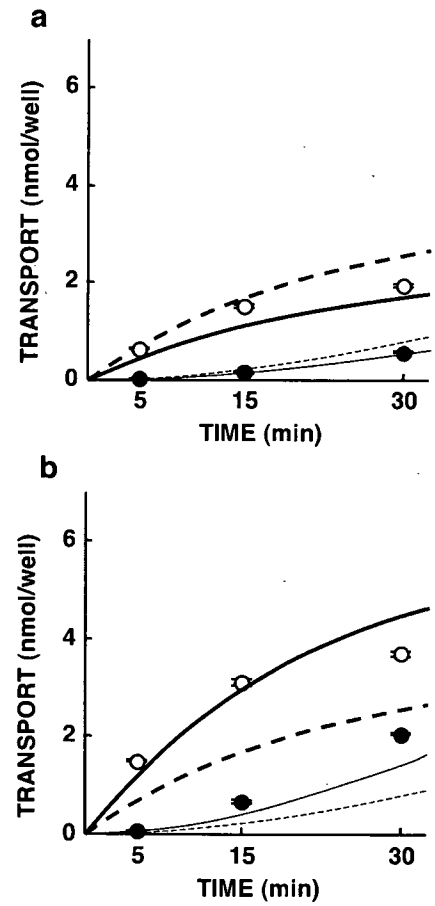

Fig. 7 Simulation of Gly-Sar transport in two clones. The accumulation and the transepithelial transport of 20 μM Gly-Sar in clone 1 (**a**) and in clone 9 (**b**) in the absorptive direction were simulated using the expanded computational model. The curves were delineated using the values of Gly-Sar transport calculated every 0.01 min with a program written in Visual Basic.NET. Numeric integration is based on Euler's method. The *bold* and *fine curves* represent the simulated accumulation and the transepithelial transport of Gly-Sar, respectively. The *solid* and *broken curves* display the simulation by the expanded and the previous models for Gly-Sar transport, respectively. The *symbols* represent the experimental data of the accumulation (*circle*) and the transepithelial transport (*filled circle*) of [^{14}C]Gly-Sar

Simulation for transepithelial transport of Gly-Sar

Based on the above findings, we chose the amount of PEPT1 mRNA as an index for the intensity of the transport activity of PEPT1. In the previous model, the maximal velocity (V_{max}) of PEPT1 in the influx direction was estimated using the parental Caco-2 cells and was defined as a constant value [11]. To incorporate mathematically the amount of PEPT1 mRNA to the simulator as a relative factor of PEPT1 activity, the V_{max} of PEPT1 in the influx direction was regarded as a variable using the following equation: $V_{max\,PEPT1,\,uptake} = 4.164 \times mRNA/1.073$ where "4.164" is the V_{max} value (nmol/min per milligram of protein) determined in the previous study [11] and "1.073" is the mean of PEPT1 mRNA (amol/μg total RNA) expressed in the parental Caco-2 cells in this study. $V_{maxPEPT1,\,uptake}$ represents the V_{max} value after correction (nmol/min per milligram of protein), and mRNA stands for the amount of mRNA (amol/μg total RNA) in the cells compared.

To validate the model, Gly-Sar transport in clones 1 and 9 was simulated using both the previous model and the improved model. The mean of the amount of PEPT1 mRNA expressed in clones 1 and 9 was 0.712 and 1.963 (amol/μg total RNA), respectively. As shown in Fig. 7, the simulation using the model developed in this study corresponded more closely with experimental data than that using the previous model, indicating that the improved model can achieve a change in the expression level of PEPT1.

Discussion

It has been proposed that computational modeling can provide a tool for the reproduction and understanding of physiological and molecular biological phenomena in which multiple factors participate [5, 9, 15, 22]. Because of the diversity and multispecificity of drug transporters, the behavior of a drug is complicated; therefore, computational modeling of drug transporters will be useful in predicting drug behavior and in studying the relationship and contribution of transporters.

Recently, based on a detailed examination of the functional properties of PEPT1 and the basolateral peptide transporter, we constructed a mathematical model of Gly-Sar transport in Caco-2 cells [11]. This model could predict Gly-Sar transport, but could not achieve a change in the expression level of PEPT1. With respect to various drug transporters including PEPT1, the expression levels of transporters were proven to affect the pharmacokinetic properties of substrates [8, 18, 20]. Furthermore, it has been demonstrated that the expression levels of PEPT1 in the small intestine differ among the segments [17] and that PEPT1 is regulated by a variety of factors [2]. Therefore, to establish a simulator of drug absorption, it is essential that the model encompasses an alteration in PEPT1 expression. To address this issue, the V_{max} value of PEPT1 is defined as a variable reflecting the expression level and is described mathematically using the amount of PEPT1 mRNA in this study. With this improved model, Gly-Sar transport in cloned cells expressing the lowest and the highest levels of PEPT1 was predicted more accurately than with the previous model (Fig. 7), indicating that our model can simulate the behavior of Gly-Sar in Caco-2 cells even if the expression level of PEPT1 is altered.

Chu et al. [4] demonstrated that PEPT1 protein expression and cephalexin uptake exhibited a good correlation using Caco-2 cells expressing PEPT1 at various levels. Furthermore, they also found that PEPT1 protein expression was well-correlated with PEPT1 mRNA level, although the data were not shown. Consistent with their report, a correlation between the transport activity and the mRNA expression of PEPT1 was confirmed in cells isolated from the parental Caco-2 cells in this study. These results suggest that the amount of PEPT1 mRNA is an appropriate index for a mathematical description of the PEPT1 expression level when a change in the activity of PEPT1 accompanies that in the PEPT1 gene expression. Besides transcriptional regulation, it has been reported that several signals, such as insulin [25] and leptin [3], induce an alteration in the PEPT1 protein expression without any change in the amount of PEPT1 mRNA. The mechanism of insulin and leptin regulation was suggested to be increased trafficking of the PEPT1 proteins from the cytoplasmic pool to the apical membranes. Because of inconvenience and difficulty, however, the determination of absolute PEPT1 protein expression level seems to be unavailable as an index of PEPT1 expression for improvement of the simulator. Therefore, we chose the expression of PEPT1 mRNA as an index and incorporated it into our model. Further studies and new technologies are needed to overcome problems in the handling of regulation that do not parallel alterations in the PEPT1 mRNA expression.

It was observed that the activity of [^{14}C]Gly-Sar uptake in clone 4 was comparable to that in the parental Caco-2 cells in spite of the higher expression of PEPT1 mRNA. In addition, more dispersion was observed in the analysis of the correlation between the activity and the mRNA expression of PEPT1 in this study compared to the previous study [4]. These differences may be caused by used cells: Chu et al. [4] used PEPT1-overexpressed Caco-2 cells established by an adenoviral transfection system, whereas we used clones isolated from the parental Caco-2 cells. It is possible that not only the expression of PEPT1 but also that of other molecules affecting the apparent activity of Gly-Sar uptake (such as Na^+/H^+ exchanger 3) [13] differ from that of the clones. Likely, several factors (other than PEPT1) among the parental cloned cells may be responsible for the slight disagreement in the simulation using the improved model with experimental data (Fig. 7). These findings suggest that, besides PEPT1, other factors should be described mathematically and incorporated into the model.

In conclusion, to adjust the previous model for the simulation of Gly-Sar transport in accordance with a change in the expression level of PEPT1, the V_{max} value of PEPT1 in the influx direction was defined mathematically using the

amount of PEPT1 mRNA as an index of the PEPT1 expression level. The improved model could well reproduce the transport of Gly-Sar in the cells expressing PEPT1 at the highest and the lowest levels. These findings suggest that our model can predict Gly-Sar transport even when PEPT1 is expressed at a different level and that the developed model may underlie a simulator for the prediction of drug absorption in the small intestine.

Acknowledgements This work was supported, in part, by the Leading Project for Biosimulation, the 21st Century COE Program "Knowledge Information Infrastructure for Genome Science," and a Grant-in-Aid for Scientific Research from the Ministry of Education, Culture, Sports, Science, and Technology of Japan. Megumi Irie is a Research Fellow of the Japan Society for the Promotion of Science.

References

1. Adibi SA (1997) The oligopeptide transporter (Pept-1) in human intestine: biology and function. Gastroenterology 113:332–340
2. Adibi SA (2003) Regulation of expression of the intestinal oligopeptide transporter (Pept-1) in health and disease. Am J Physiol Gastrointest Liver Physiol 285:G779–G788
3. Buyse M, Berlioz F, Guilmeau S, Tsocas A, Voisin T, Péranzi G, Merlin D, Laburthe M, Lewin MJM, Rozé C, Bado A (2001) PepT1-mediated epithelial transport of dipeptides and cephalexin enhanced by luminal leptin in the small intestine. J Clin Invest 108:1483–1494
4. Chu X-Y, Sánchez-Castaño GP, Higaki K, Oh D-M, Hsu C-P, Amidon GL (2001) Correlation between epithelial cell permeability of cephalexin and expression of intestinal oligopeptide transporter. J Pharmacol Exp Ther 299:575–582
5. Clancy CE, Rudy Y (1999) Linking a genetic defect to its cellular phenotype in a cardiac arrhythmia. Nature 400:566–569
6. Daniel H (2004) Molecular and integrative physiology of intestinal peptide transport. Annu Rev Physiol 66:361–384
7. Daniel H, Kottra G (2004) The proton oligopeptide cotransporter family SLC15 in physiology and pharmacology. Pflugers Arch 447:610–618
8. Hashida T, Masuda S, Uemoto S, Saito H, Tanaka K, Inui K (2002) Pharmacokinetic and prognostic significance of intestinal MDR1 expression in recipients of liver-donor liver transplantation. Clin Pharmacol Ther 69:308–316
9. Hoffmann A, Levchenko A, Scott ML, Baltimore D (2002) The IκB–NF-κB signaling module: temporal control and selective gene activation. Science 298:1241–1245
10. Inui K, Yamamoto M, Saito H (1992) Transepithelial transport of oral cephalosporins by monolayers of intestinal epithelial cell line Caco-2: specific transport systems in apical and basolateral membranes. J Pharmacol Exp Ther 261:195–201
11. Irie M, Terada T, Okuda M, Inui K (2004) Efflux properties of basolateral peptide transporter in human intestinal cell line Caco-2. Pflugers Arch 449:186–194
12. Irie M, Terada T, Sawada K, Saito H, Inui K (2001) Recognition and transport characteristics of nonpeptidic compounds by basolateral peptide transporter in Caco-2 cells. J Pharmacol Exp Ther 298:711–717
13. Kennedy DJ, Leibach FH, Ganapathy V, Thwaites DT (2002) Optimal absorptive transport of the dipeptide glycylsarcosine is dependent on functional Na^+/H^+ exchange activity. Pflugers Arch 445:139–146
14. Leibach FH, Ganapathy V (1996) Peptide transporters in the intestine and the kidney. Annu Rev Nutr 16:99–119
15. Matsuoka S, Sarai N, Kuratomi S, Ono K, Noma A (2003) Role of individual ionic current systems in ventricular cells hypothesized by a model study. Jpn J Physiol 53:105–123
16. Motohashi H, Sakurai Y, Saito H, Masuda S, Urakami Y, Goto M, Fukatsu A, Ogawa O, Inui K (2002) Gene expression levels and immunolocalization of organic ion transporters in the human kidney. J Am Soc Nephrol 13:866–874
17. Naruhashi K, Sai Y, Tamai I, Suzuki N, Tsuji A (2002) Peptl mRNA expression is induced by starvation and its level correlates with absorptive transport of cefadroxil longitudinally in the rat intestine. Pharm Res 19:1417–1423
18. Pan X, Terada T, Irie M, Saito H, Inui K (2002) Diurnal rhythm of H^+-peptide cotransporter in rat small intestine. Am J Physiol Gastrointest Liver Physiol 283:G57–G64
19. Saito H, Inui K (1993) Dipeptide transporters in apical and basolateral membranes of the human intestinal cell line Caco-2. Am J Physiol Gastrointest Liver Physiol 265:G289–G294
20. Sakurai Y, Motohashi H, Ueo H, Masuda S, Saito H, Okuda M, Mori N, Matsuura M, Doi T, Fukatsu A, Ogawa O, Inui K (2004) Expression levels of renal organic anion transporters (OATs) and their correlation with anionic drug excretion in patients with renal diseases. Pharm Res 21:61–67
21. Sawada K, Terada T, Saito H, Inui K (2001) Distinct transport characteristics of basolateral peptide transporters between MDCK and Caco-2 cells. Pflugers Arch 443:31–37
22. Schoeberl B, Eichler-Jonsson C, Gilles ED, Müller G (2002) Computational modeling of the dynamics of the MAP kinase cascade activated by surface and internalized EGF receptors. Nat Biotechnol 20:370–375
23. Terada T, Inui K (2004) Peptide transporters: structure, function, regulation and application for drug delivery. Curr Drug Metab 5:85–94
24. Terada T, Sawada K, Saito H, Inui K (1999) Functional characteristics of basolateral peptide transporter in the human intestinal cell line Caco-2. Am J Physiol Gastrointest Liver Physiol 276:G1435–G1441
25. Thamotharan M, Bawani SZ, Zhou X, Adibi SA (1999) Hormonal regulation of oligopeptide transporter Pept-1 in a human intestinal cell line. Am J Physiol Cell Physiol 276: C821–C826
26. Thwaites DT, Brown CDA, Hirst BH, Simmons NL (1993) Transepithelial glycylsarcosine transport in intestinal Caco-2 cells mediated by expression of H^+-coupled carriers at both apical and basal membranes. J Biol Chem 268:7640–7642
27. Thwaites DT, Brown CDA, Hirst BH, Simmons NL (1993) H^+-coupled dipeptide (glycylsarcosine) transport across apical and basal borders of human intestinal Caco-2 cell monolayers display distinctive characteristics. Biochim Biophys Acta 1151:237–245
28. Vachon PH, Beaulieu J-F (1992) Transient mosaic patterns of morphological and functional differentiation in the Caco-2 cell line. Gastroenterology 103:414–423
29. Yang CY, Dantzig AH, Pidgeon C (1999) Intestinal peptide transport systems and oral drug availability. Pharm Res 16:1331–1343

Pharmaceutical Research, Vol. 23, No. 4, April 2006 (© 2006)
DOI: 10.1007/s11095-006-9665-2

Research Paper

Androgen Receptor is Responsible for Rat Organic Cation Transporter 2 Gene Regulation but not for rOCT1 and rOCT3

Jun-ichi Asaka,[1] Tomohiro Terada,[1] Masahiro Okuda,[1] Toshiya Katsura,[1] and Ken-ichi Inui[1,2]

Received October 18, 2005; accepted December 7, 2005

Purpose. Organic cation transporters 1–3 (OCT1–3; Slc22a1–3) mediate the membrane transport of organic cations in the kidney. We previously reported that rat (r)OCT2 expression in the kidney was regulated by testosterone. In this study, we examined the transcriptional mechanisms underlying the testosterone-dependent regulation of rOCT2 expression.
Methods. Approximately 3000-bp fragments of the rOCT1–3 promoter region were isolated, and promoter activities were measured in the renal epithelial cell line LLC-PK_1 with the coexpression of rat androgen receptor.
Results. Among reporter constructs tested, only rOCT2 promoter activity was stimulated by testosterone. This stimulation was suppressed by nilutamide, an antiandrogen drug. Reporter assays using deletion constructs and mutational constructs of putative androgen response elements (ARE) in the rOCT2 promoter region suggested that two AREs, located at approximately −3000 and −1300, respectively, play an important role in the induction by testosterone.
Conclusions. Testosterone induces the expression of rOCT2, but not of rOCT1 and rOCT3, via the AR-mediated transcriptional pathway. This is the first study to address the transcriptional mechanisms of testosterone-dependent gene regulation of the Slc22 family.

KEY WORDS: gender difference; kidney; promoter; rOCT2; testosterone.

INTRODUCTION

Proximal tubules play important roles in the renal elimination of drugs. Cationic drugs are secreted from blood to urine by combined efforts of two distinct classes of organic cation transporters: one driven by the transmembrane electrical potential difference in the basolateral membranes, and the other driven by the transmembrane H^+ gradient in the brush-border membranes (1). Molecular cloning studies identified three kinds of organic cation transporters (OCT1–3), and their physiological and pharmacokinetic roles have been evaluated (2,3). Rat (r)OCT1 (Slc22a1) is expressed abundantly in the liver and kidney (4), whereas rOCT2 (Slc22a2) is expressed in the kidney, but not in the liver (5). These transporters are localized to the basolateral membranes of renal proximal tubules (6,7). rOCT3 (Slc22a3) is expressed predominantly in the placenta, and also in the intestine, heart, brain, lung, and very weakly in the kidney (8). Functional studies using heterologous expression systems revealed that all OCTs recognized a variety of organic cations with different molecular structures including tetraethylammonium, 1-methyl-4-phenylpyridinium, N^1-methylnicotinamide, choline, and dopamine (8,9).

It was reported that the uptake of tetraethylammonium was greater in renal cortical slices of male rats than female rats (10), suggesting gender differences in the basolateral membrane transport activity for organic cations. We found that expression level of rOCT2, but neither rOCT1 nor rOCT3, in the kidney was much higher in males than females and suggested that rOCT2 is responsible for gender differences in renal basolateral membrane organic cation transport activity (11). Furthermore, we demonstrated that treatment of male and female rats with testosterone significantly increased rOCT2 expression in the kidney (12). These results suggested that testosterone plays a pivotal role in the transcriptional regulation of the rOCT2 gene. However, no information has been available to demonstrate this process.

Androgens, such as testosterone, are main hormones responsible for the male phenotype (13). As with other steroid hormones, many effects of androgen are mediated by a specific intracellular androgen receptor (AR; NR3C4). AR activated by testosterone binds to the androgen response element (ARE) in the 5′-flanking region of target genes and is responsible for the expression of various genes such as the C3 subunit of prostatin (14) and prostate-specific antigen gene (15). Based on our previous studies, we hypothesized that AR could be involved in the regulation of the rOCT2 gene.

[1] Department of Pharmacy, Kyoto University Hospital, Faculty of Medicine, Kyoto University, Sakyo-ku, Kyoto 606-8507, Japan.
[2] To whom correspondence should be addressed. (e-mail: inui@kuhp.kyoto-u.ac.jp)

ABBREVIATIONS: AR, androgen receptor; ARE, androgen response element; bp, base pair; CYP, cytochrome P450; DMEM, Dulbecco's modified Eagle's medium; FBS, fetal bovine serum; MMTV, mouse mammary tumor virus; OCT, organic cation transporter; PCR, polymerase chain reaction; RACE, rapid amplification of cDNA ends.

In the present study, therefore, we examined the effects of testosterone on the promoter activities of rOCTs to understand the role of this hormone in the gender differences of rOCT2 expression.

MATERIALS AND METHODS

Materials

Restriction enzymes were obtained from New England BioLabs (Beverly, MA, USA). T4 kinase and T4 DNA ligase were purchased from TaKaRa (Ootu, Japan). [α-^{32}P] CTP was obtained from Amersham Biosciences, Inc. (Buckinghamshire, UK). Testosterone was purchased from Nacalai Tesque (Kyoto, Japan). Nilutamide was obtained from Sigma (St. Louis, MO, USA).

Determination of Putative Transcriptional Start Sites

The putative transcriptional start sites for rOCT1-3 were determined by 5′-rapid amplification of cDNA ends (5′-RACE) using the rat Marathon-Ready cDNA kit (Clontech, Palo Alto, CA, USA) according to the manufacturer's instructions. The rOCT2 gene-specific primers for the 5′-RACE were designed and synthesized based on the genomic sequence. The 5′-RACE was performed with adapter primer 1 that came with the kit and a gene-specific primer of rOCT1 (accession number NM_012697), 5′-CACAACCAGGGAGCCCAGGAAGAAG CCC-3′ (538 to 511). Nested polymerase chain reaction (PCR) was performed with adapter primer 2 and a nested gene-specific primer of rOCT1, 5′-CAGGAAGGCTTGTTTCTGGAAC CAGCCA-3′ (106 to 79). The rOCT2 gene-specific primers are as follows: a gene-specific primer of rOCT2 (accession number NM_031584), 5′-CCTTCATAAGAGGTTGTTAA GCCTGCCACTGGA-3′ (605 to 577); a nested gene-specific primer of rOCT2, 5′-GGAGGCACCAGACAGCAGGCT AAGAGG-3′ (187 to 160). The rOCT3 gene-specific primers are as follows: a gene-specific primer of rOCT3 (accession number NM_019230), 5′-GCCCAGGAAGACCACACCAA CGAAGAG-3′ (520 to 493); a nested gene-specific primer of rOCT3, 5′-GTCAGGCACAGCAGCAGGAACACGCG CC-3′ (474 to 450).

Genomic Cloning of rOCT1, rOCT2, and rOCT3 Promoters

rOCT1 and rOCT3 promoters were isolated from the rat genome (Clontech) by a PCR-based method using the following primers designed based on the rat genomic DNA (accession number AC114389): rOCT1 sense 5′-GGACGCGTCCA TGCTCTGCGAACTGAGGT-3′ and antisense 5′-GGCTC GAGGACTGCCACCAGGGGTTCAT-3′; rOCT3 sense 5′-GGACGCGTCCCTTCGAAGCAGAGGGAAAA-3′ and antisense 5′-GGAGATCTTGCAGGAATAGCCTCCAGT GC-3′. On the other hand, the rOCT2 promoter was isolated from the rat genomic library (Clontech) with a conventional plaque hybridization method. The probe was prepared by PCR using rat genomic DNA (Clontech) as a template. The primers, designed based on the rat genomic DNA (accession number AC114389), were as follows: 5′-GGCTTGGGAGAT GGCTAAGTA-3′ and 5′-TCACAGCCATGTGGGACA TGT-3′. Phage DNA with a long rOCT2 promoter was prepared with a QIAGEN lambda midi kit (Qiagen, Hilden, Germany) and partially sequenced. The transcription factor-binding sites were predicted with TRANSFAC 5.0 software (http://www.gene-regulation.com/cgi-bin/pub/programs/match/bin/match.cgi?), with a core similarity of 0.95 and a matrix similarity of 0.90.

Construction of Reporter Gene and Rat Androgen Receptor Expression Plasmid

Approximately 3-kb fragments corresponding to the 5′-flanking regions of the rOCT genes were subcloned into a pGL3-Basic luciferase gene vector (Promega, Madison, WI, USA) to yield rOCT1 (−3025/+23), rOCT2 (−3036/+242), and rOCT3 (−3001/+31). The deletion constructs rOCT2 (−1895/+242), rOCT2 (−819/+242), rOCT3 (−1095/+31), and rOCT3 (−515/+31) were prepared with the restriction enzymes. The mouse mammary tumor virus (MMTV) gene excised from pMSG (Amersham Biosciences) was subcloned into pGL3 to yield MMTV-pGL3.

ARE mutants were constructed using QuikChange® II Site-Directed Mutagenesis Kit (Stratagene, La Jolla, CA, USA) according to the manufacturer's instructions. Primer sequences are listed in Table I.

Table I. Sequences of Mutation Primers

Primer	Sequence
ARE-1 S	5′-GGCCTCTGTGGTAGAGGA**GCC**ACTTAATCTTGCTGC-3′
ARE-1 AS	5′-GCAGCAAGATTAAGTGGCTCCTCTACCACAGAGGCC-3′
ARE-2 S	5′-CCTATGAGGACCAAGC**GCC**ACTCTCATGTCCTTCCTG-3′
ARE-2 AS	5′-CAGGAAGGACATGAGAGTGGCGCTTGGTCCTCATAGG-3′
ARE-3 S	5′-CCTTGGCACAGGA**GCC**TCTCCTTGACTCTCACCTG-3′
ARE-3 AS	5′-CAGGTGAGAGTCAAGGAGAGGCTCCTGTGCCAAGG-3′
ARE-4 S	5′-GCGTCCTGATACAGAC**GCC**ACCCATGAGTCAGTCAC-3′
ARE-4 AS	5′-GTGACTGACTCATGGGTGGCGTCTGTATCAGGACGC-3′
ARE-5 S	5′-CAGCAGGAAAGAGAGACTACC**GCC**TTCCCTGGCATTTGG-3′
ARE-5 AS	5′-CCAAATGCCAGGGAAGGCGGTAGTCTCTCTTTCCTGCTG-3′

Underlined sequences are putative ARE sequences, and bold characters indicate positions of the ARE mutation.
ARE = androgen response element.

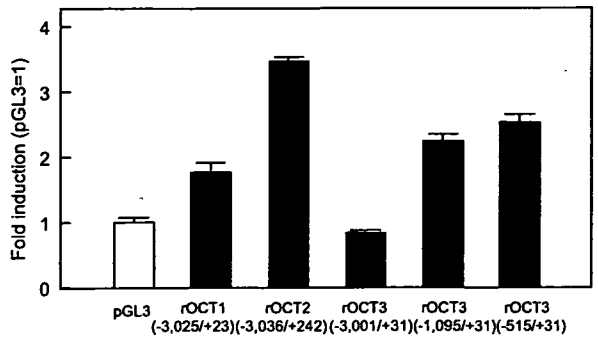

Fig. 1. Promoter activities of rat organic cation transporter (rOCT) genes. rOCT1–3 promoter constructs were transfected into LLC-PK_1 cells for luciferase assays. Firefly luciferase activity was normalized to *Renilla* luciferase activity. Each column represents the mean ± SE of three independent experiments.

cDNA for rat AR (rAR: accession number, NM_012502) was isolated from rat kidney cDNA by a PCR-based method using the following primers: sense 5′-GGGATCCAGGATG GAGGTGCAGTTAGGG-3′ (991 to 1011) and antisense 5′-GGCTCGAGTTTCCAAATCTTCACTGTGTG-3′ (3713 to 3693). PCR was performed using Pfu polymerase (Stratagene) as follows: 95°C for 3 min; 35 cycles of 95°C for 1 min, 60°C for 1 min, 72°C for 8 min; and a final extension at 72°C for 10 min. The PCR product was subcloned into the expression vector pBK-CMV (Stratagene).

Cell Culture and Luciferase Assay

The porcine kidney epithelial cell line LLC-PK_1 was obtained from American Type Culture Collection (ATCC CRL-1392; Rockville, MD) and cultured as described previously (16). For the luciferase assay, the cells were seeded at 1.5×10^5 cells into 24-well plates in Dulbecco's modified Eagle's medium (DMEM), supplemented with 10% charcoal-stripped fetal bovine serum (FBS). Cells were transfected by 5-h exposure to LipofectAMINEplus (Invitrogen Japan KK, Tokyo, Japan), with each well containing 0.6 μg of the rOCT2 (−3036/+242) or equimolar amount of other reporter constructs, 0.1 μg of the rAR expression vector, and 30 ng of an internal control vector for transfection efficiency, namely, the *Renilla* luciferase (pRL-TK) reporter plasmid (Promega) in serum-free DMEM. The medium was changed to DMEM supplemented with 10% charcoal-stripped FBS, containing testosterone, nilutamide, or the vehicle control, dimethyl sulfoxide. After 43-h incubation, the cells were harvested and lysed, and luciferase activity was determined using a dual luciferase assay kit (Promega) and a LB940 luminometer (Berthold, Bad Wildbad, Germany). Each reporter construct was assayed in triplicate wells, and each experiment was repeated three times.

Statistical Analysis

The data were expressed as the mean ± SE. The significance of differences between the vehicle-treated and testosterone-treated groups was analyzed using Dunnet's *post hoc* analysis. Other analyses were conducted with Student's *t* test. Significance was set at $p < 0.05$.

RESULTS

Determination of the Transcriptional Start Site(s) for rOCTs in Rat Kidney Using 5′-RACE

The transcriptional start site(s) for rOCTs in the rat kidney were identified using 5′-RACE. The putative transcriptional start sites were determined using the longest RACE product. Sequencing of the amplified bands revealed that the terminal position of rOCT1 cDNA with the longest 5′-untranslated region was located 63 nucleotides above the start codon, which is 26 bp upstream of the 5′-end of rOCT1 cDNA reported previously (4). The terminal position of rOCT2 cDNA was located 306 nucleotides above the start codon, which is 266 bp upstream of the 5′-end of rOCT2 cDNA (5). The terminal position of rOCT3 cDNA is 35 nucleotides above the start codon, which is 359 bp downstream of the 5′-end of rOCT3 cDNA (8). Therefore, the terminal position of

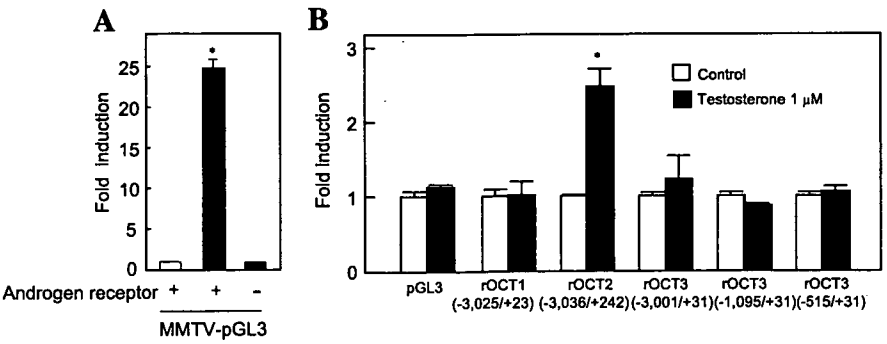

Fig. 2. (A) *Trans*-activation of the mouse mammary tumor virus (MMTV) promoter by rat androgen receptor (rAR) in the presence of testosterone. (B) *Trans*-activation of rOCT1–3 promoters by rAR in the presence of testosterone. Constructs were transiently transfected into LLC-PK_1 cells with rAR and pRL-TK. The cells were cultured for 43 h with vehicle or 1 μM testosterone, and luciferase activity was measured. Firefly luciferase activity was normalized to *Renilla* luciferase activity. Each column represents the mean ± SE of three independent experiments. $^*p < 0.05$, significantly different from control.

rOCT cDNA with the longest 5′-untranslated region was numbered with +1 as the transcription start site in this study.

Isolation and Analysis of 5′-Flanking Region of rOCT Genes

Based on the transcriptional start site, we then isolated the promoter region (about 3 kb) of each transporter and prepared reporter constructs. For luciferase assay, we used LLC-PK_1 cells because LLC-PK_1 cells possessed organic cation transport activities (16,17) and pig organic cation transporter OCT2p (18). Figure 1 shows the basal promoter activities of each transporter in LLC-PK_1 cells. Reporter constructs for rOCT1 and rOCT2 showed significant promoter activity. A reporter construct for rOCT3 (−3001/+31) did not have promoter activity, but those for rOCT3 (−1095/+31) and rOCT3 (−505/+31) did, suggesting that a repressive region is located in the rOCT3 promoter region −3001 to −1095. These findings suggest that all promoter constructs function appropriately.

Using these constructs, the effects of testosterone on the promoter activities were assessed. The functional activity of rAR was confirmed by a reporter assay using MMTV reporter construct in the presence of 1 μM testosterone (Fig. 2A). AR has been shown to *trans*-activate MMTV promoter using testosterone (19). In the absence of rAR, MMTV promoter activity was not enhanced by testosterone; native AR was not expressed in LLC-PK_1 cells. As shown in Fig. 2B, the activity of the rOCT2 promoter was significantly enhanced by testosterone, but that of the rOCT1 and rOCT3 promoters was not. These results were consistent with our previous results of Northern blotting (11). We therefore further characterized the transcriptional mechanisms by which the rOCT2 promoter is stimulated by testosterone.

Figure 3 shows the nucleotide sequence for 1000 bp upstream of the translation start site of the rOCT2 gene. Putative binding sites for many transcription factors were identified by TRANSFAC with a core similarity of 0.95 and a matrix similarity of 0.90, including activating protein (AP)-1, octamer-binding factor (Oct)-1, HNF-3/Fkh Homolog (HFH)-3, and a CCAAT box.

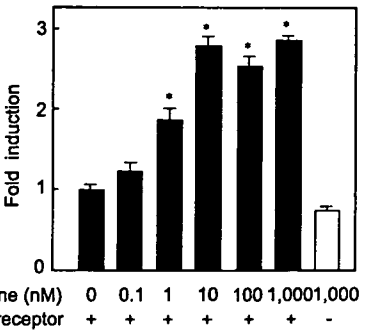

Fig. 4. *Trans*-activation of the rOCT2 promoter (−3036/+242) by rAR in the presence of testosterone. Constructs were transiently transfected into LLC-PK_1 cells with rAR and pRL-TK. The cells were cultured in the presence or absence of testosterone for 43 h. The vector pBK-CMV was used instead of rAR, and luciferase activity was measured. Firefly luciferase activity was normalized to *Renilla* luciferase activity. Each column represents the mean ± SE of three independent experiments. $*p < 0.05$, significantly different from 0 nM testosterone.

Region of 5′-Flanking Sequence Required for Response to Testosterone

As shown in Fig. 4, a reporter construct for rOCT2 (−3036/+242) was significantly activated by testosterone in a concentration-dependent manner, and about a 3-fold increase was observed with 10 nM testosterone. Testosterone did not activate the rOCT2 promoter construct in the absence of the rAR expression vector. Nilutamide, an antiandrogen drug, acts as a competitive inhibitor of the androgen receptor (20). Nilutamide blocked the activation of the rOCT2 promoter by testosterone in a dose-dependent manner (Fig. 5), but nilutamide is a partial agonist of androgen receptor; rOCT2 activity is not completely suppressed by nilutamide. These findings suggest that rOCT2 promoter activity is stimulated by AR. Therefore, we tried to identify ARE(s) that work to stimulate rOCT2 promoter activity.

Table II shows sequences, positions, and homology to the consensus sequence of ARE within the 3000 bp of rOCT2

```
-694 GGAAGGGGGAAAGAGAGAGGAAGGCGGGGGACACACAGAAGACAGACAGATTTACATTCCAGTTTTATAATGCAGGTTTGTCAGCAGGCTACCCCCGTCT -595
                                                  Oct-1                                          HFH-3
-594 TTGTTTTGCTTGGCAGCATCAGTATGCTCTGGGATCCTTCTGTCCAGCAGGAAAGAGAGACTACCTGTTTCCCTGGCATTTGGATACCCTTAGCAGCATC -495
                          Hand1/E47
-494 CTGAAGGAGCATCCCTAAGTTAGATGGAACAACCTGGAACAACGGAATGACAGTAGAACAAATACACCCATGTCCTGCGTTTGCACTTGACCTATATGTA -395

-394 AGGCAAATGTGGTACTCTTTCCTCACAAGGGGGTGAAGAGGAAGGACACATCAGGGTTGAGAGGTAAGAATGCTAAACTGGAATGAACCCTTGGAAACGT -295
                                                                                                RFX-1
-294 CAGACTGATTCAATCTGAGAGAAATCAAAGCACGCCGCCACAGCATGTCGCTCAAGTGCATCGCTTTCAGGGGGATTCAGGAGCTTGGATCCAGGACCCC -195
       AP-1                                                Nkx2-5
-194 CCAGACCCTGATGCAAATTGCACTGGGTGTGTATAACCAAGTGCGCGTGTGTCTGTGTCACACCTACAAGAGAGGCTGGCTGTGTAGGTAACAAGGATAT -95
            Oct-1                                N-Myc
-94  ATTAATTTTCTGGCCACTTAATGTGCTAGGGAAAGATTAACCAGCTGTGATATGTTAAGAGACTCAGATTTCTCCCCGTGGGATACAGAGAAGTGATTGT +6
          CCAAT box                                                                                    ▲
+7   TTGTAGTGCTGCTGTGAGGCAGAGACAAACTCACAGAGAATGAGGTTACAATAAACACATCACACTCCAGGGCCTGCTCTGGGCATTTCCGGGCAGCAAG +106
                                                                                                NF-κB
+107 ATCTTCCCCCATTGGAGAGAGGTGCGATTGGAAGTTGGCCTGTCCGAGGGACGTCTGACCCAAAGGCTGGTCCCTCTCTAAATAAGCTAATGCTCACCCT +206
                                                                                  AP-1
+207 TTGACTCTTGGTCAAGAGTCATCCTGAGCTGAGCGCGCTGCCTTCAGCAGCATTTGGAGCCCTGTGGGTGAAGCCTCAGGAACAGCTGCCTCCAGGGACC +306
                          Δ
```

Fig. 3. Transcriptional elements of the rOCT2 promoter. A 1000-base genomic DNA sequence immediately upstream of the start codon site is listed. An open triangle indicates the putative transcriptional start position, and a closed triangle indicates the 5′-end of rOCT2 cDNA published so far (NM_031584).